MXene-Based Composites and Their Applications

Prakash Krishnaiah, Hafiz Taimoor Ahmed Awan, Rashmi Walvekar, and Sivakumar Manickam

Abstract MXenes have received remarkable attention due to their outstanding physical and chemical properties. They exhibit exceptional tunable performance due to their 2D structure and rich functional group, making them easy to combine with other materials such as polymers, metal oxides, 2D chalcogenides, carbonaceous, and organic hybrid materials to meet the high-performance requirements. Furthermore, MXenes and their composites have shown outstanding electrical, mechanical, and optical properties due to their functional groups and surface chemistry. This chapter covers the synthesis, surface mechanism, and applications of MXenes and related composites. For a better understanding, we address the fundamentals of MXenes to their associated fabrication techniques, including HF etching, exfoliation delamination, in-situ polymerisation, hydrothermal, etc. Then, applications of MXenes are discussed, such as energy storage in supercapacitors, batteries, solar cells, and sensors. Moreover, EMI shielding performance, water remediation, and catalytic activity of MXene/composite are highlighted. In the last part, the challenges and prospects of the MXenes and composites have been addressed to evaluate the general complications, problems, and possible solutions of the materials during synthesis and applications.

P. Krishnaiah
Centre for Nano and Material Sciences, Jain Global Campus, Jain University, Kanakapura, Bangalore 562112, India

H. T. A. Awan
Graphene and Advanced 2D Materials Research Group (GAMRG), School of Engineering and Technology, Sunway University, No. 5, Jalan Universiti, Bandar Sunway, 47500 Petaling Jaya, Selangor, Malaysia

R. Walvekar
Department of Chemical Engineering, School of Energy and Chemical Engineering, Xiamen University Malaysia, Jalan Sunsuria, Bandar Sunsuria, 43900 Sepang, Selangor, Malaysia

S. Manickam (✉)
Petroleum and Chemical Engineering Department, Faculty of Engineering, Universiti Teknologi Brunei, Bandar Seri Begawan 1410, Brunei Darussalam
e-mail: manickam.sivakumar@utb.edu.bn

© The Author(s), under exclusive license to Springer Nature Switzerland AG 2022

M. Khalid et al. (eds.), *Fundamental Aspects and Perspectives of MXenes*,
Engineering Materials, https://doi.org/10.1007/978-3-031-05006-0_4

Keywords Two-dimensional materials · MXene · Metal oxides · Polymers · Chalcogenides · Composite materials · Energy storage

1 Introduction

Two-dimensional (2D) materials have been intensively researched recently owing to their large specific surface area, high catalytic behavior, highly tunable wide-bandgap, etc. 2D materials have two dimensions outside the nanoscale range [1]. The quest to develop 2D nanostructured materials has accelerated since Novoselov and Geim discovered graphene in 2004 [2]. The 2D family encompasses a diverse range of materials, including graphene, silicene, borophene, transition metal oxides, layered double hydroxides (LDH), and MXenes, as well as hybrid materials and composites based on 2D materials [3–5]. MXenes, a unique 2D material developed in 2011 by Gogotsi and Barsoum [6]. MXenes belong to the transition metal carbides, nitrides and carbonitrides and are synthesized by the selective etching of 'A' layers from their MAX phases that have a general formula $M_{n+1}AX_n$, where n = 1, 2 or 3; M stands for transition metals like (Ti, Ta, Nb, Zr, Cr, Mo, V or Mn) while A represents IIIA and IVA group elements (Al, Si, Ga, Ge, Sn, In, Pb or As), and X can be both carbon and nitrogen elements [7].

The newly synthesized 2D materials, MXenes, are obtained by losing A layers from their original MAX phase, and their 2D nature is identical to that of graphene. It was reported that during the etching process, the surfaces of $M_{n+1}X_n$ units are always covered with functional groups such as oxygen, hydroxyl (–OH) and/or fluorine (–F). Hence, the chemical formula of MXenes is represented as $M_{n+1}X_nT_x$, where T_x shows the surface functional groups in MXenes [8]. The multifaceted chemistry of MXenes with interesting mechanical, electronic, magnetic, and electrochemical properties make them special among 2D materials. 2D morphological features with layered structures and high flexibility make MXene a suitable filler material for generating different composite materials, providing an opportunity to assimilate the tremendous properties of several 2D materials in a complementary manner. Because of this, MXenes and MXene related composites have also drawn significant attention to the scientific community in recent years for many applications. MXenes and MXene-based composites materials primarily found applications in energy storage as excellent-performance electrode materials for sodium (Na)-ion batteries, lithium-sulfur (LiS) batteries, and supercapacitors because of their splendid electrochemical performance and greater conductivity [9–11].

Besides its metal oxides, polymers and hybrid materials also play a vital role in the region of physical sciences, such as physics, chemistry, material sciences, and a variety of applications. The oxide materials acquire the broad composition of structural geometries and electronic structures, yielding to its insulator, metallic and semiconductor specification [12–15]. Oxide particles have exhibited distinctive physical and chemical characteristics due to their large density and small particle size [16]. These oxides materials include Al_2O_3, V_2O_5, TiO_2, Fe_2O_3, CeO_2 and

many more [17–23]. Furthermore, polymers and hybrid materials are the formation and combination of two or more materials and compounds (organic and inorganic) having large macromolecules and repeat ting of large molecular chain because of its identical chemical amalgamation of particles. These kinds of hybrid materials are mostly present under the scale range of 1 μm which helps these materials for the sort of various composites of this scale range [24–26]. These materials are the combination of many polymers associated with cold mixture and precondensate. Hybrid materials also exhibit many excellent properties such as chemical resistance, acid toughness, surface adhesion, rapid changing of room temperature, corrosion resistance etc. [27–30]. These polymers and hybrid materials include polysulfides, polyesters, polyurethanes, alkyds, cellulose, polyvinyl alcohol and others [31–36].

This chapter is divided into five sections; each section will cover the comprehensive details of 2D materials based on MXenes, and their composite with metal oxides, polymers, carbonaceous material, chalcogenides and hybrid materials. Furthermore, every section contains tabular information on Mxenes and their composite, including their comprehensive properties, specific parameters, and, most importantly, their applications. Various types of applications mentioned in this section include supercapacitors, batteries, sensors, photocatalysis, solar cells, thermal, dielectric, EMI shielding, bio medicines, aerospace, and many other energy-related applications [37–43].

2 Metal Oxide Doped MXene Composites

With the growing need for smart, compact, wearable, and stretchable electronic items, it is essential to develop suitable rechargeable energy storage devices that are inexpensive to manufacture, resulting in less pollution and increased safety [44, 45]. MXene displays an outstanding electrical conductivity and unique layered structure, enabling it as an attractive supporting material for many metal-ion based battery applications. Xu et al. [46] prepared vanadium pentoxide/MXene ($V_2O_5{\cdot}nH_2O/Ti_3C_2T_x$) composite as a cathodic material for zinc-ion batteries with a simple hydrothermal method. They reported a significant enhancement of electrochemical performance with the addition of MXene into metal oxide (V_2O_5), mainly due to the smart 3D structure of MXene that facilitates the high charge transport and effectively accommodates the zinc ion insertion/desertion with outstanding structural modifications.

Song et al. [47] proposed incorporating MXene composites with manganese oxide (MnO_x) for lithium-sulfur batteries. Figure 1 shows the synthesis of MnO_x/MXene composites and mechanism of their alteration of polysulfides on MnO_x/MXene. Composites of metal oxides with MXene act as chemically active support for the interaction between MnOx and MXene, significantly increasing the oxygen vacancy in the MnO_x materials. The stronger support interaction of oxide between MXene and MnO_x boosted the higher adsorption of polysulfides, and their modification occurred in the cathode. The higher adsorption and conversion of polysulfides formed

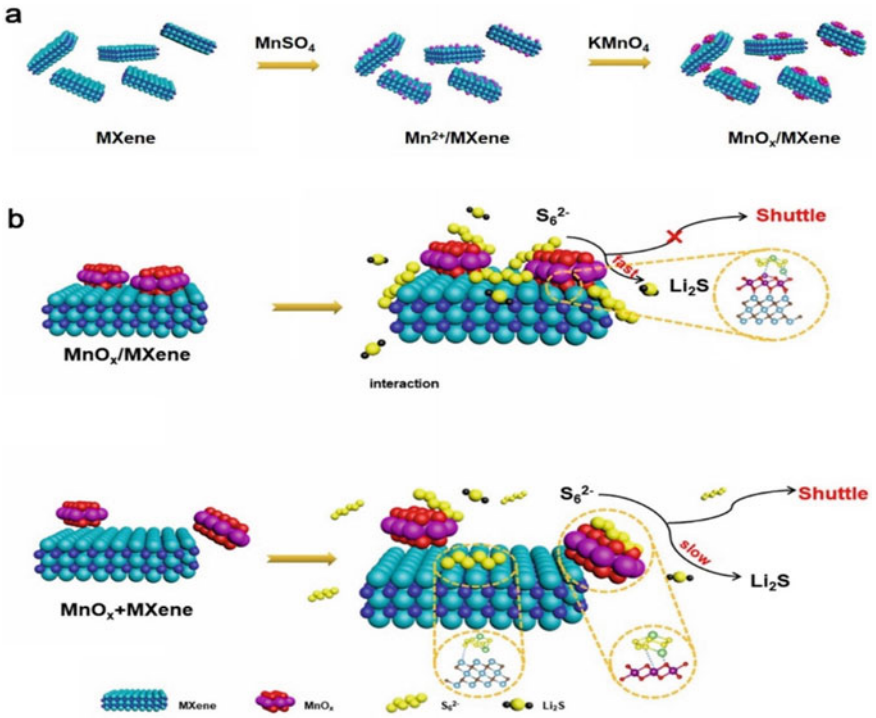

Fig. 1 Synthesis of MnO_x/MXene composites (**a**); the mechanism of conversion of polysulfides on MnO_x/MXene (**b**) [47] (reproduced with permission)

on the cathode surface overcome their loss due to diffusion, leading to enhanced electrochemical performance and stability.

It is well-known that metal oxide-based electrode materials, especially transition metal oxides, have attracted researchers by their easy synthesis in large scale and rich redox reactions, contributing to higher specific capacitance than many carbon-based materials. However, their poor dimensional stability and inherent semi-conductive properties lead to lower specific capacitance and rate capability after a few hundred cycles [48].

Due to excellent stability, rich surface-active sites and the pseudocapacitive contribution of MXene and their composites with different metal oxides have been largely attracted. Wu et al. [49] synthesized nanosheets of heterostructured $NiCo_2S_4$ composites decorated with ultrathin MXene sheets for advanced electrode material in supercapacitors. They found that the surface-functionalized MXene composites (N-Ti_3C_2/$NiCo_2S_4$) showed exceptional electrochemical properties with a specific capacitance of 1879 $F.g^{-1}$, which is far better than the pristine metal oxides or MXenes. They also noticed that the materials retained the cycling stability of 76.3%

even after 5000 cycles, demonstrating remarkable stability. This is mainly due to N-$Ti_3C_2/NiCo_2S_4$ composites with significant specific surface areas, accessible hierarchical 2D structure, and good contact with the electrolyte, allowing more charge/ions transport networks. Huang et al. [50] proposed nanobelt like metal oxide into MXene to prepare sandwich and layered structured composites composed of growing belt-like structure of amorphous $Na_{0.23}TiO_2$ on the surface of MXene sheets. The as-prepared $Na_{0.23}TiO_2$/MXene composite was utilized as a LIB anode electrode material. They reported that the composite material gave impressive cycling life and excellent rate capability. The discharge capacity of the material exhibited an upward trend with the enhancement in continuous 4000 charge–discharge cycles. The excellent stability and rate capability even after 4000 cycles are attributed to a sandwich-like structure with nanobelt of MXene composites that lowers the transfer of ions and successfully releases the electrode strain upon cycling.

Besides the electrode material, metal-oxide doped MXene composites are increasingly used in other important applications such as catalysis, EMI shielding, electromagnetic wave absorption, coatings, sensors, etc. Yin et al. [51] introduced a self-assembled sandwich-like structure of $Cu_2O/TiO_2/Ti_3C_2$ composites which showed outstanding catalytic properties for the degradation of nitro compounds. Generally, the catalytic degradation rate of nitro compounds is used to determine the catalytic properties of any material (Fig. 2).

In $Cu_2O/TiO_2/Ti_3C_2$ composites, no catalytic activity was found in the presence of TiO_2/Ti_3C_2, which clearly shows that the Ti_3C_2 and TiO_2/Ti_3C_2 were failed to perform catalytic degradation of nitro compounds. This occurs due to the poor electrical conductivity of TiO_2, limiting its catalytic activity. However, $Cu_2O/TiO_2/Ti_3C_2$ with the optimized quantity of Cu_2O showed excellent catalytic properties. Cu_2O enables the easy transport of electrons from an electron donor such as $NaBH_4$ to TiO_2 through the surface of Ti_3C_2 (MXene). They also found that the ternary composites ($Cu_2O/TiO_2/Ti_3C_2$) show excellent dimensional stability by more than 92% efficiency after 8 cycles. The main reason for the exceptional stability was due to the larger specific surface area of MXene composite (TiO_2/Ti_3C_2),

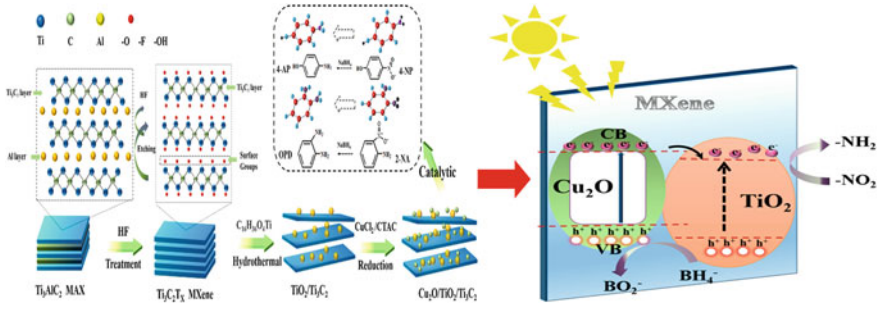

Fig. 2 Synthesis of MXene composites ($Cu_2O/TiO_2/Ti_3C_2$) and their mechanism of catalytic degradation of nitro compounds [51] (reproduced with permission)

enabling Cu_2O to adhere to the surface. Hou et al. [52] synthesized Co_9S_8 decorated MXene hybrid composites using a simple hydrothermal and high-temperature carbonization technique. The as-prepared MXene metal oxide hybrid composites ($Co_9S_8/C/Ti_3C_2T_x$) exhibited excellent electromagnetic (EM) wave absorption properties. MXene composites showed good storage capacity of EM waves and exhibited significant dissipation of EM waves, indicating improved dielectric characteristics of the composite material. The hybrid material of MXene composites with good impedance matching with EM waves makes it easier to dissipate within the material instead of reflection (Fig. 3).

The multilayered composites with many interfaces between MXene and metal oxide increase the loss of conductivity and formation of interfacial polarization, leading to excellent dissipation of EM waves. Liu et al. [53] introduced indium oxide (In_2O_3) nanocubes into MXene composites to examine the methanol gas sensing application at ambient temperature. The In_2O_3 nanocubes decorated MXene composite showed outstanding gas sensing characteristics compared to other pristine metal oxides or pristine MXene. The $In_2O_3/Ti_3C_2T_x$ composites exhibited gas sensitivity from 5 to 100 ppm of methanol concentration within 6.5 s and 3.5 s of response time and recovery time, respectively. This is an outstanding gas sensing performance compared to other gas sensing materials. Comparatively, $In_2O_3/Ti_3C_2T_x$ composites illustrated excellent gas sensitivity because of the unique and large mesoporous surface area of MXenes, enabling the accumulation of many oxygen molecules that significantly improved the sensor response and selectivity. A huge number of hidden functional groups, like −O, −OH, and −F etc., within the multilayered MXene material act as active sites for the adsorption of methanol molecules. The possible mechanism of gas sensing application of $In_2O_3/Ti_3C_2T_x$ as proposed by the authors is shown in Fig. 4.

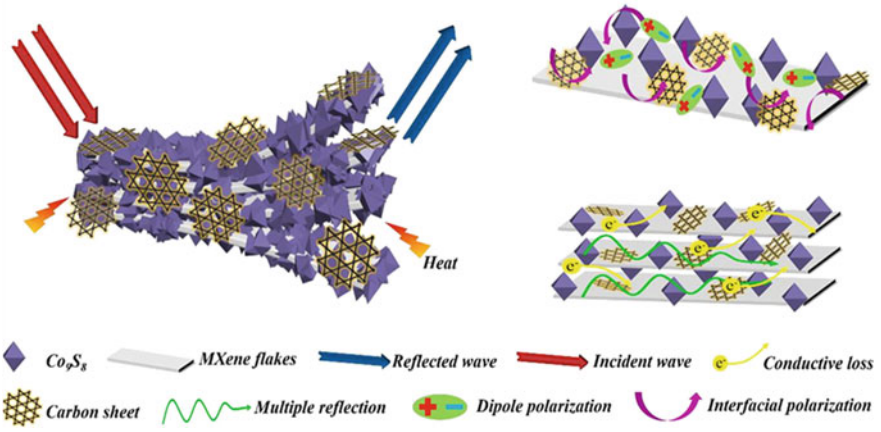

Fig. 3 Schematic representation of the possible mechanism of electromagnetic absorption of MXene composites ($Co_9S_8/C/Ti_3C_2T_x$) [52] (reproduced with permission)

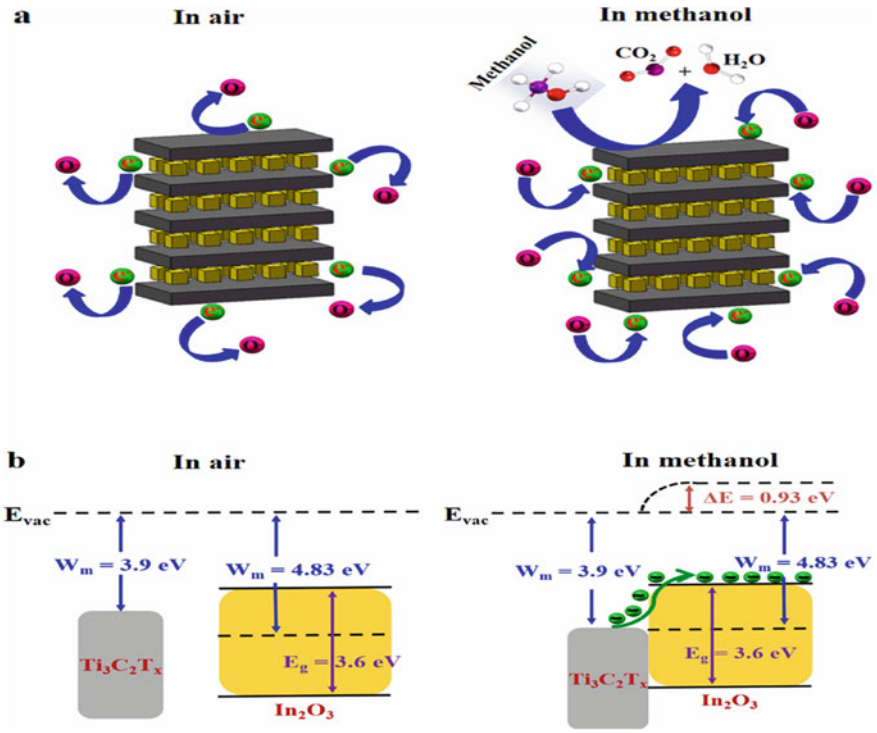

Fig. 4 Possible mechanism of gas sensitivity (**a**) and energy band diagram (**b**) of $In_2O_3/Ti_3C_2T_x$ composites in air and methanol [53] (reproduced with permission)

Similarly, Zhang et al. reported the CoO_x-NiO incorporated with MXene nanosheets prepared via atomic layer deposition route for the potential energy storage supercapacitor applications [54]. The synthesized device based on CoO_x-$NiO/Ti_3C_2T_x$ MXene nanosheet achieved the specific capacitance of 1960 F/g along with the cyclic life of 90.2% after the 8000 cycles. Liu et al. mentioned the MXene composite with rGO and CuO hybrid aerogel for sensing technology. The as prepared MXene/rGO/CuO materials obtained excellent acetone sensing performance at ambient temperature and recorded the 52.09% acetone response toward the 100 ppm [55]. The reported metal oxides to generate composites with MXenes are mainly transition metal oxides, showing excellent properties for various applications such as the battery, supercapacitor, sensing, catalysis, coating, etc. and have illustrated superior performance than their pristine materials as mentioned in Table 1.

Lin et al. [66] proposed a simple method to synthesise a novel 2D photocatalytic composite membrane of $Bi_2O_2CO_3$@MXene with multi-functional material that enables efficient water treatment. They showed that the MXene composite membrane has ultrahigh water flux due to incorporating nitrogen-doped $Bi_2O_2CO_3$ nanoparticles. The MXene composite membrane helps increase the adsorption of dye molecules by electrostatic interaction. The presence of negatively charged functional

Table 1 Describes the MXene and MXene doped oxide and its composite materials according to its potential applications and measuring parameters

S. no	MXenes	Oxides	Measuring parameters	Applications	References
1	$Ti_3C_2T_x$	$LiMn_2O_4$	243 F g^{-1} capacitance 88% life span	Supercapacitors	[56]
2	$Ti_3C_2T_x$	TiO_2	2650 $\mu molh^{-1}g_{cat}^{-1}$	Photocatalysis	[57]
3	Ti_3C_2	SnO_2	126 F g^{-1} capacitance 82% capacity retention	Supercapacitors	[58]
4	Ti_3C_2	TiO_2	43 $\mu molh^{-1}g_{cat}^{-1}$	Photocatalytic activity	[59]
5	$Ti_3C_2T_x$	MnO_2	212 F g^{-1} capacitance 88% cyclic life	Supercapacitors	[60]
6	N-Ti_3C_2	Fe_2O_3	1065 mAh g^{-1} Specific capacity	Li-Ion batteries	[61]
7	N-$Ti_3C_2T_x$	RGO	1180 mAh g^{-1} specific capacity 82.5% capacity retention	Li-Sul batteries	[62]
8	$Ti_3C_2T_x$	RGO hybrid aerogel	23.3 Sm^{-1} electrical conductivity 27.3 dB EMI shielding effect	EMI shielding	[63]
9	$Ti_3C_2T_x$	Metal/ZnO/MXene and Metal/ZnO: Pd/MXene	19,400 nm RIU^{-1} and 8350 nm RIU^{-1} sensitivities	SPR biosensors	[64]
10	$Ti_3C_2T_x$	FTO/TiO_2/$MAPbI_3$	13.83% efficiency	Perovskite solar cell	[65]

groups on the surface of the MXene can adsorb cationic dyes. Moreover, the presence of specific hydroxyl groups and the large specific surface area of MXene play a major role in its adsorption capacity. The sponge-like MXene nanocomposites were synthesized with Gd^{3+} doped vanadium oxide (GVO/MXene) to degrade industrial effluents and pathogens [67]. As compared to the undoped vanadium oxide (VO), the GVO/MXene nanocomposites showed outstanding dye degradation performance of 92% due to the presence of Gd^{3+} and MXene nanosheets in the nanocomposites. Gd^{3+} in the composites improve the light harnessing photodegradation. In addition to this, the high surface area and a large number of active sites on the surface of the MXene enhances the photodegradation ability of GVO/MXene nanocomposites. The GVO/MXene nanocomposites also show superior inhibition of bacterial growth in the presence of GVO/MXene nanocomposites as compared to VO nanoparticles.

3 Polymer-MXene Composites

Polymer-based materials are broadly utilized in our day-to-day life due to their remarkable performance and comfortable processing. In contrast, a single polymer cannot satisfy a range of intended applications. Recent developments in nanotechnology offer solutions for developing composite materials based on polymers with other nanofillers with excellent physical and thermal properties. Significant attempts have been made to tune polymer composites' thermal and mechanical properties by changing the type of filler. In recent years, MXene has been a widely used filler material in the preparation of polymer composites. Due to the excellent hydrophilic surfaces, mechanical properties, and metallic conductivity of MXenes, polymer composites with MXenes could achieve highly enhanced mechanical and thermal properties. It is also reported that incorporating many terminal active sites on the surface of MXenes during etching can increase the correlation between MXene flakes and polymer chains, offering a suitable environment for manufacturing high-performance MXene/polymer composites [68].

Furthermore, MXene possesses covalent and metallic bonds from the bonding point of view, which further tunes the conductive properties and bandgap in the MXene structure. Similarly, the existence of the defect on the MXene surface may advance the charge mobility of the MXene [69–71]. On the other hand, Polymer and MXene contain nanofiller that possess covalent bonding. Hydrogen (H) bonding can also interact with MXene, which assists uniformly and firmly dispersed among the MXene and polymer composite materials and helps create the 3D structure of MXene-polymer. Such as, the composite of MXene with xanthan yielded the hydrophilic polysaccharide $(C_6H_{10}O_5)_n$ with −O functional group was utilized to fabricate this material. Due to the strong H-bonding amidst xanthan and MXene, the MXene can be uniformly divided in the xanthan matrix [72]. Besides it's the oxygen (−O) and hydroxyl (−OH) functional group on surface MXene made the MXene surface negatively (−ve) charged, which yields to make the strong bond, i.e., positive (+ve) charged polymers, like polyethyleneimine and poly-diallyldimethylammonium chloride through an electrostatic interaction [35].

MXene incorporated polymers led to different types of composite materials such as laminated composites/structure [73], MXene coated polymeric fiber [74], composite fiber [75], aerogel, foam/sponge [76], spin-coated electrospun fiber membranes [77], etc. Generally, the preparation methods of composite materials are highly influenced by their end-use applications. Till now, multiple varieties MXene and polymer-based composite materials have been prepared due to synergetic outcomes of inorganic and organic MXene and polymers, respectively. The solution blending technique is commonly used to prepare thin-film types of composites involving the dissolution of both fillers and the polymer in a solvent. The composite materials are formed after mold pouring and evaporation of solvent. To obtain the good dissolution of polymer and filler, thorough stirring is required during solution casting process. Solution blending is the preferred method for the synthesis of MXene-polymer composites due to excellent hydrophilicity of MXene and is also

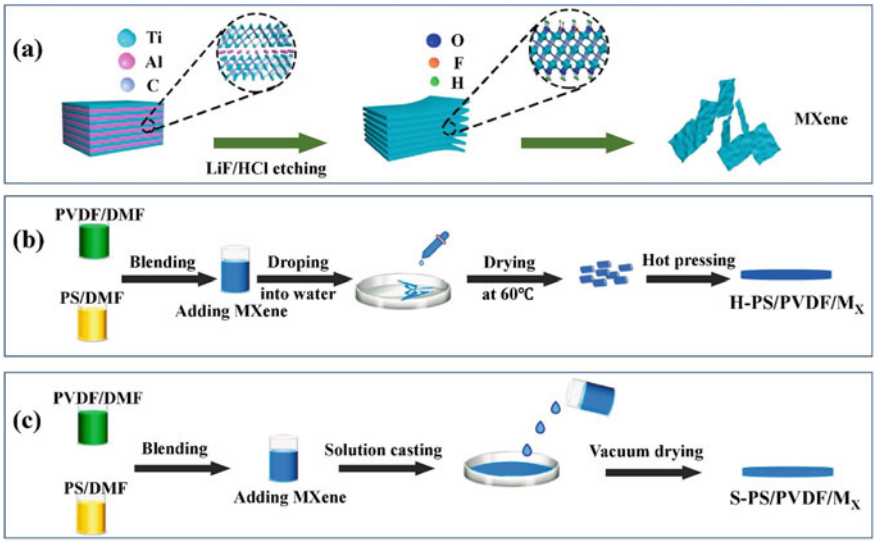

Fig. 5 Preparation methods for $Ti_3C_2T_x$ (MXene) nanosheets and their polymer composites [79] (reproduced with permission)

easy and flexible to manage filler and polymer ratio which improves the dispersion between MXene and polymer [78]. A typical solution blending method for the synthesis of MXene/PS/PVDF hybrid polymer composites is shown in Fig. 5.

Jin et al. [80] synthesized poly(vinyl alcohol) (PVA)/MXene multilayered films by solution blending method. This alternative arrangement of MXene and PVA multilayered and continuous thin films is excellent for the conduction of heat and electrons, which endows excellent electromagnetic interference (EMI) shielding and thermal conductivity. Liu et al. [81] used solution casting and vacuum-assisted filtration to synthesize MXene/chitosan films to apply for high-performance EMI shielding. Vacuum-assisted filtration was the best method to achieve the required thickness of MXene/Chitosan films and well-aligned MXene sheets on chitosan. The maximum shielding effect can be achieved due to tunable film thickness, aligned nanosheet structure, and outstanding metallic conductivity. The 37-micron thick MXene/chitosan at a $T_3C_2T_x$ content of 50% reached the specific shielding effectiveness to 15,153.9 ± 153 dB/cm, which outperformed the testified biomass-based EMI shielding composites in the X-band frequency. In most cases, it is necessary to adopt multi fabrication techniques such as solution blending and melt blending to achieve excellent dispersion and reduce agglomeration [82]. Melt blending is a highly preferred fabrication method for preparing high-performance polymer composites where high mechanical, thermal and flame-retardant properties are required due to their excellent dispersion and low agglomeration of nanofillers (Fig. 6).

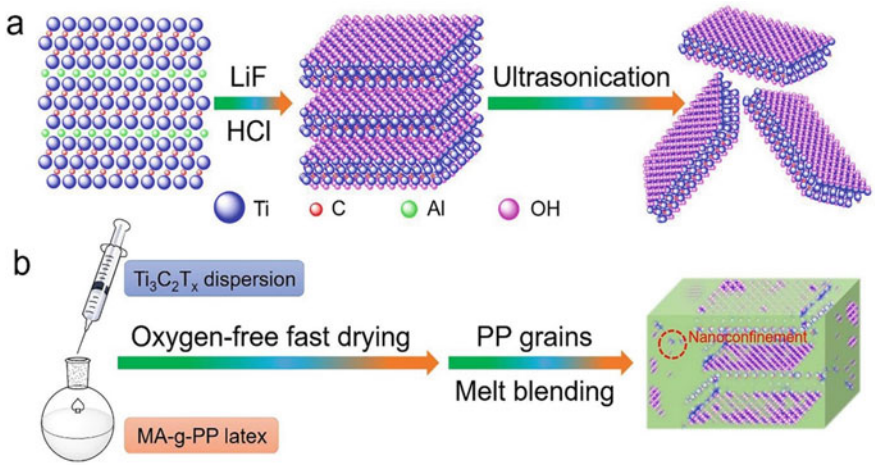

Fig. 6 Schematic diagram exhibiting the fabrication of MXene and preparation of MXene/PP composites by melt blending [82] (reproduced with permission)

Ming-Ke Xu et al. reported the $Ti_3C_2T_x$ MXene/polypropylene (PP) nanocomposite for highly effective EMI shielding [83]. The nanocomposite yielded an electrical conductivity of 437.5 C/cm along with the EMI shielding effect of 60 dB, confirming the tremendous performance of this material. Xue et al. [84] reported the fabrication of Polyphosphoramide (PPDA)-intercalated MXene incorporated polylactide (PLA) biocomposites with excellent mechanical, thermal and flame retardant properties. They found that the combination of PPDA and MXene filled PLA composites showed good flame retardant and excellent mechanical properties. This is mainly because of the homogeneous dispersion of PPDA and MXene nanofillers across the PLA matrix, offering effective load transfer and enabling fracture energy dissipation when the external load is applied to the matrix. The major advantage of using MXene as a filler in any polymer matrices is its enormous negative charge sites across the MXene surface. These charged sites and functional groups of polymer surface can form an interlinked network, leading to efficient transportation of electron and load transfer, resulting in excellent electrical conductivity and improved mechanical and thermal properties [85, 86].

Like graphene oxide, vast numbers of functional groups on the surface of MXene nanosheets present higher possibilities to interlink between nanosheets and polymer matrices, leading to improved mechanical properties. A larger number of hydrogen bonds on the surface of MXene nanosheets and polymer matrices easily form rigid and cross-linked networks between them, leading to significantly improved thermal, mechanical, and flame retardant properties of the resultant polymer composites [87]. Zhao et al. [88] demonstrated that rich hydroxyl groups bonding together in MXene and PVA made it possible to get highly stable and flexible polymer composites. They found that the tensile modulus significantly increased by 100 times for adding 30% MXene into PVA compared with pristine MXene thin film (2.87 MPa). This is

highly significant since elastic modulus was calculated based on interfacial cross-linking between filler and polymer. When the delaminated MXene nanosheet was chemically blended with PVA, the hydrogen bonds were formed with the surface functional groups of polymer matrix and MXene nanosheets, which enhanced the interfacial binding energy (BE) to increase the mechanical properties of resultant composites. In addition, the unchanging dispersion of d-Ti_3C_2 in polyvinyl alcohol was helpful to increase the intermolecular forces to further enhance the mechanical properties of MXene-polymer composites. Zhou et al. prepared the nanocellulose polymer mixed with MXene with the help of the spray coating technique [89]. The nanocellulose nanofiber and MXene composite were employed for the EMI shielding effect and electro-photothermal performance. The synthesized Ti_3C_2 MXene/cellulose nanofiber, when tested, it yields a mechanical strength of more than 250 MPa, excellent desirable toughness of 20 Mj/cm^3 and EMI effect of 60 Db. Similarly, Shi et al. [82] developed a high-performance polymer composite relying on PP and MXene inspired by natural 3D networks such as silkworm net, honeycomb and spider web. They used solution casting followed by melt blending to fabricate ultra-thin 2D nanocomposites of PP and MXene. They reported that the tensile strength of MXene/PP composites enhanced with increasing the loading of MXene. This is mainly due to hydrogen bonding between PP polymer and MXene filler, hindering the free mobility of the polymer chains and causing an enhancement in the tensile properties of the composites as compared to pristine polymer. By adding 2 wt% Mxene nanosheets, they achieved an increase of 35.3%, 674.6% and 102.2% in the tensile strength, ductility and modulus, respectively. A large number of hydrogen bonds induced nanoconfinement is responsible for the increased mechanical properties. However, elongation at break reduced with a small loading of MXene filler and then significantly increased mainly due to bond slippage in the interface of filler and polymer and reduced number of hydrogen bonds due to the agglomeration of filler. In in-situ polymerization tactic, the mixture containing polymer precursors, fillers and curing agents (or initiators) are initially premixed in solutions, and then it polymerized to create macromolecules under specific conditions. The major advantage of this technique is that good dispersion of functionalized nanoparticles could be achieved within the polymer matrices [90]. Carey et al. synthesized MXene/Nylon-6 nanocomposites by in situ ring-opening polymerization of ε-caprolactam and achieved well-exfoliated nanocomposites with significantly improved water transporting properties of the resultant nanocomposites. Due to the rapid growth of technology, adopting conventional manufacturing methods brings huge challenges to end-use applications. Hence, it is necessary to think out of the box to utilize the unlimited potential of materials properties to convert them into required end-use applications. Zheng et al. [91] reported a unique particle construction strategy called heterogeneous agglomeration to fabricate highly conductive and stable MXene incorporated polystyrene (PS) composites (MXene/PS composites), where PS emulsion converted into uniform sized 3D microspheres (PS particles), and MXene sheets were then incorporated into PS particles (Fig. 7). MXene nanosheets were completely filled between the PS particles along with strong adsorption of MXene sheets on the surface of PS particles during the strong suction filtration process, enabling strong orientation of MXene

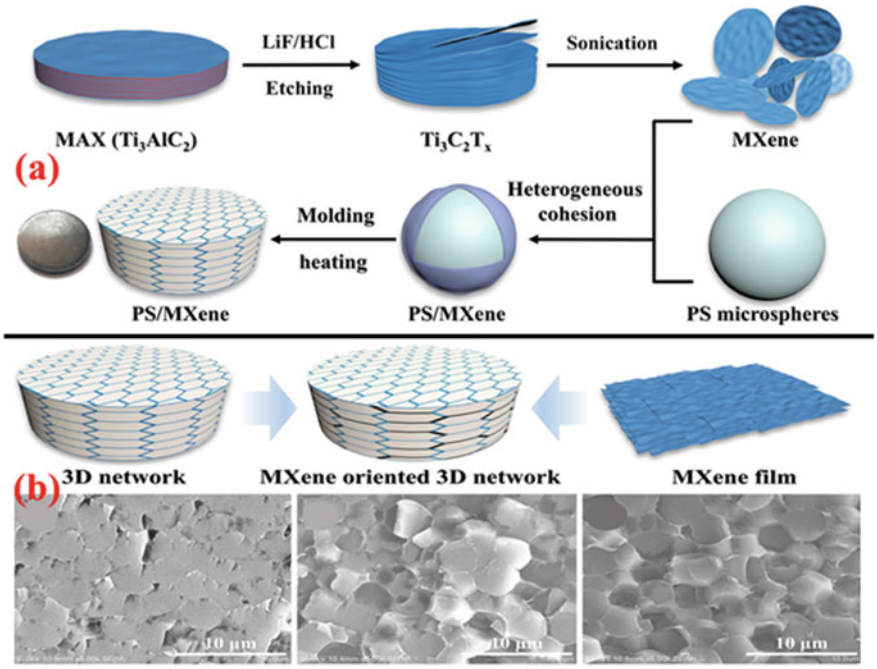

Fig. 7 Synthesis of MXene (**a**) and schematic illustration of MXene oriented 3D network structure and their cross-sectional SEM image of polystyrene composites (**b**) [91] (reproduced with permission)

sheets within the composites. This strong orientation of MXene nanosheets across the polymer composites drastically enhanced the resultant composite's mechanical, physical, thermal, and electrical performance. Due to the efficient and well-ordered structure of MXene/PS composites, the conductivity increased significantly to 3846.15 S m^{-1} with the addition of just 1.81% of MXene filler. The obtained conductivity is significantly higher than other PS composites reported so far. The flame-retardant and EMI shielding nanocoatings onto cotton fabrics were applied by layer-by-layer self-assembled technology using tannic acid modified MXene synthesized P, N-co-doped cellulose nanocrystals (TA-Mxene and PA@PANI@CNC) [92]. The resultant nanocoatings show that cotton fabric's EMI shielding efficiency (SE) with 20 bilayers coatings (Cotton-20BL) reaches up to 21 dB over the X- band frequency range. Moreover, the Cotton-20BL reaches an excellent limited oxygen index of 32. More importantly, the peak heat release rate and total smoke production are reduced by 63.0% and 98.3%, respectively. As compared to pristine cotton fabrics, the high absorbance intensities of flammable volatiles and toxic gas, including carbonyl compounds, aliphatic ethers, CO and CO_2, are markedly reduced due to the nanobarrier effect of 2D MXene and catalytic carbonization effect of PA. The Mxene nanocomposite coatings also shows good electrical conductivity and improve

chemical stability due to presence of 2D $Ti_3C_2T_x$ nanosheets which contribute to the dissipation of electromagnetic microwaves.

For more clarification regarding MXene and polymer materials, Table 2 describes several MXene and polymers regarding their unique characteristics, measurements values, and applications.

4 Carbon-Based MXene Composites

Numerous types of carbon-based nanomaterials like graphene oxide (GO), porous carbon (PC), carbon nanotubes (CNTs), carbon dots (CDs), fullerene, and carbon nanohorns (CNHs) have been exploited for potential applications in the areas of electronics, biology, medicine, environment, etc., owing to their unique physical and chemical characteristics [102–104]. The novelty of the material plays a vital role in the new technological advancements. Sun et al. [105] proposed a novel composite of MXene incorporated nitrogen-doped carbon foam (NCF) with 3D hallow neurons like architecture for solid-state supercapacitors. The authors claimed that the as-prepared MXene/NCF demonstrated a remarkable (332 F g^{-1}) capacitance, 3162 mF cm^{-3} volumetric capacitance of 64% rate capacity, which is more than 99% retention of its capacity after ten thousand cycles. The remarkable electrochemical performance was achieved due to the as-prepared 3D hollow interconnected neuron-like architecture with highly compressible, large specific surface area and highly flexible electrode of MXene/NCF composites. Zhao et al. [106] fabricated $Ti_3C_2T_x$-CNT composites and utilized this for ECs. As-prepared composites having $Ti_3C_2T_x$ and CNT layers were alternately deposited on top of each other until the total number of layers reached 6–10, which looked like a sandwich-like superposition of the MXene and CNT layers. The as-prepared electrode material for the supercapacitor, these layers exhibited superior volumetric capacitance and rate performance compared to pristine MXene. The volumetric capacitance of the $Ti_3C_2T_x$-CNT electrode increased from 340 F cm^{-3} to 370 F cm^{-3} after the 10,000 charge discharge cycles, and exhibits 55% rate which is much higher than as compared to $Ti_3C_2T_x$ electrode. A key reason for the outstanding electrochemical performance exhibited by the $Ti_3C_2T_x$-CNT composite is that CNT expands its interlayer space for an intercalation of cation, and therefore enhances the diffusion paths for electrolyte ions.

Zhou et al. [107] used V_2C and Mo_2C based MXenes, and nitrogen-doped graphene to obtain MXene/graphene composites and used them as hydrogen evolution reaction (HER) and bifunctional electrocatalysts for oxygen reduction reaction (ORR. They noticed that a minimal overpotential for ORR could be as low as 0.3 V, including a kinetic barrier of 0.2 eV. The HER process had free energy of hydrogen adsorption ($\Delta GH*$) close to one, and the reaction barrier to Tafel was as low as 1.3 eV. Graphene heterostructures exhibit favorable properties due to the strong electron transition between the MXene and graphitic sheet, altering the graphene band profile and the band center relative to the Fermi level.

Table 2 MXenes and their composite materials according to their potential applications and measuring parameters

S. no	MXenes	Polymer	Measuring parameters	Applications	References
1	$Ti_3C_2T_x$	Polypyrrole	9.5 mF/cm^2 capacitance 250 mWh/cm^3 energy density	Micro-supercapacitors	[93]
2	$Ti_3C_2T_x$	PVA	17–716 S m^{-1} electrical conductivity 0.1–4.5 W m^{-1} K^{-1} thermal conductivity	EMI shielding and thermal conductive	[94]
3	$Ti_3C_2T_x$ carbon nanotube	Polycaprolactone	30–50 mF/cm^2 areal capacitance	Flexible energy storage	[77]
4	d-Ti_3C_2	PVC	11,800 dielectric constant 3.48 W m K^{-1} thermal conductivity	Dielectric properties	[95]
5	Ti_3C_2	PANI	164 F g^{-1} specific capacitance	Supercapacitors	[96]
6	$Ti_3C_2T_x$	PEDOT:PSS	30.8 F g^{-1} specific capacitance	Supercapacitors	[97]
7	$Ti_3C_2T_x$	PDMS/Au/Ti$_3C_2T_x$/SiO_2/*n*-Si/In:Ga	10.22% efficiency	Photovoltaic cell	[98]
8	$Ti_3C_2T_x$	PANI	−56.30 dB reflection loss	EMI shielding and microwave absorption	[99]
9	Ti_3C_2	Thermoplastic polyurethane	47.1% tensile strength 39.8% storage modulus	Thermo related industries	[100]
10	$Ti_3C_2T_x$	PVA	528 F/cm^3 volumetric capacitance	Supercapacitors	[101]

MXene/GO composites can be utilized for many potential applications owing to their good electrical conductivity and enormous specific surface area [108]. The low thermal conductivity and poor flame retardant properties of graphene have limited its potential applications, such as thermal management. Micro-processing devices are used in many modern-day electronics, tend to generate a lot of waste heat and create high energy hot spots, causing lower performance and long life of the electronic devices [109]. The combination of MXene and GO 2D materials offers thermal management in the microprocessors in many electronic devices. Wan et al. reported the 2D bi-metal (Fe-Te) oxide/carbon/$Ti_3C_2T_x$ MXene for high performance Li-ion storage [110]. The synthesized prepared material having the composition of $(Fe_{2.5}Ti_{0.5})_{1.04}O_4$/C/$Ti_3C_2T_x$ MXene obtained the 757.2 mAh/g discharge capacity after the 800 charge–discharge cycles. Liu et al. [111] reported that paper-like composite material synthesized from GO and MXene composites showed excellent thermal conductivity and flame retardant properties. The authors found that by adding 40% MXene sheets into GO, the thermal conductivity increased by 184% compared to the pristine GO. In GO, the heat conduction occurs through phonon diffusion through lattice vibrations of its covalent sp^2 hybridization. The GO sheets were thermally resistant to phonon scattering due to many surface defects and grain boundaries. However, the addition of MXene nanosheets and the reduction of GO content in the MXene/GO composite film exhibit more sp^2 hybridized carbon structure that offers effective channels for phonon migration, leading to increased thermal conductivity (Fig. 8). Concerning flame retardancy properties, the presence of a large number of hydroxyl groups on the surface of GO leads to poor flame resistance ability. However, the addition of MXene nanosheets into nanosized TiO_2 acts as an effective thermal barrier at the high-temperature flame. It assists in removing hydroxyl groups on the GO surface, leading to increased fire resistance and conversion of GO into RGO (reduced graphene oxide) [111]. The authors noticed that 40% of MXene nanosheets into GO showed an extremely low heat release rate, and char residue was 91.36%, 10 times higher than pristine GO.

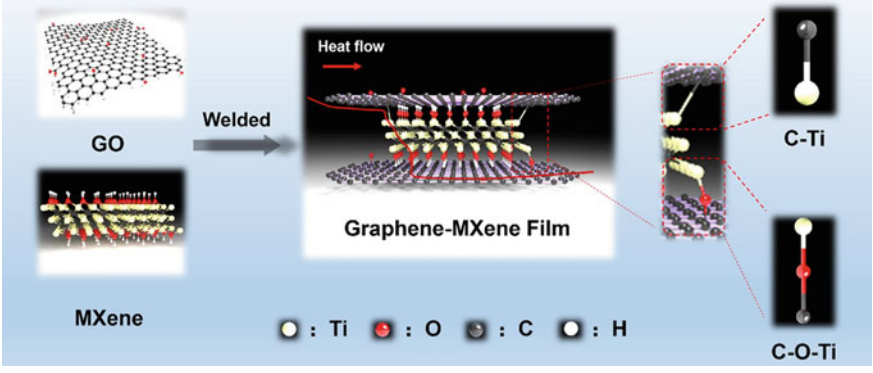

Fig. 8 Schematic representation of LED and its subsequent IR thermal image [111] (reproduced with permission)

Recently, Qi et al. reported the $Ti_3C_2T_x$ MXene composite with starch-derived carbon foam (MPCF) for thermal insulation and electromagnetic interference shielding effect [112]. The as-prepared carbonized PCF electrical conductivity of 21.8 S/cm and compression strength of 4.9 MPa at 1400 °C. Moreover, this material gained the specific shielding effect and EMI shielding effect of 216 cm^3/g and 75 dB, respectively. Aissa et al. [113] synthesized a sandwich type of composite structure using MXene and graphene nanoplatelets (GNPs) by electrohydrodynamic atomization deposition method as a potential thin film for EMI shielding applications in extremely high-frequency M-band from 60 to 80 GHz. The as-prepared thin films below 2 μm showed good electrical conductivity, outstanding electron mobility and very high EMI shielding properties. The outstanding properties of MXene/GNPs composite thin films were due to the deposition of GNPs on the surface of MXene nanosheets, creating a cross-linked conductive network across the thin film that offers extra electrons and conductive pathways within the composite layers. GNPs have also increased the electron flow of the composite film by closing pin-holes on the surface of MXene nanosheets (Fig. 9).

Friction and wear materials are becoming crucial for technological developments to reduce material losses caused by friction and wear. Few 2D materials such as molybdenum disulfide (MoS_2), graphene and graphene oxide (GO) are used in lubricant applications in the transportation and industrial sectors [114, 115]. Some reports claim that MXene is an excellent 2D solid lubricant material [116]. However, the hydrophilic nature of MXene and high reactivity towards water vapor and other gases lead to structural degradation [117]. The above problem can be overcome by incorporating other 2D materials into MXene [118]. A unique heterostructure

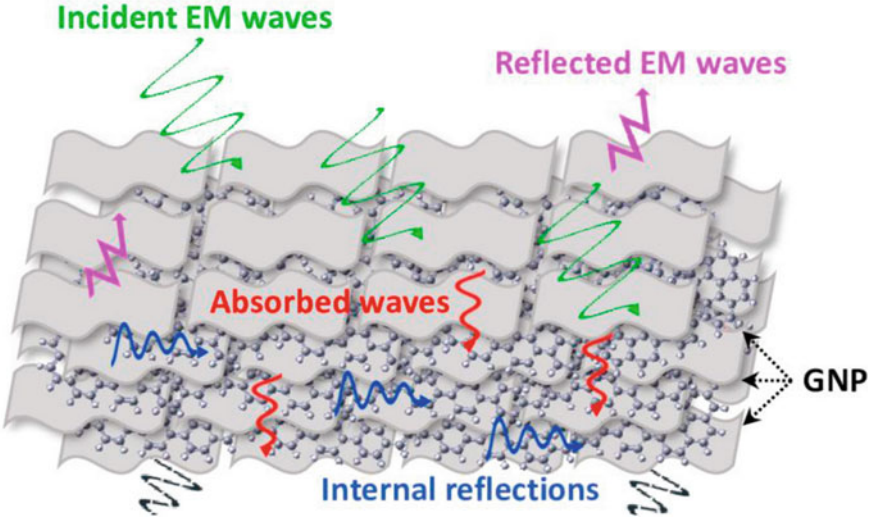

Fig. 9 Schematic representation of different governing phenomena during EMI shielding of 2D sandwiched MXene/GNPs composite thin films [113] (reproduced with permission)

can be obtained by mixing MXene nanosheets and GO. These distinctive composites of MXene/GO offer excellent tribological performance in both air and nitrogen atmosphere. Apart from individual merits of MXene and GO, the heterostructure of MXene/GO coating displayed improved stability at dry nitrogen atmosphere due to their existence of continuous and even distribution of composite layers [119]. Huang et al. [118] introduced MXene/graphene coatings to achieve superlubricity under a nitrogen atmosphere. They coated MXene/graphene composite on SiO_2 coated silicon (Si) substrate and subjected to wear by sliding against diamond-like carbon-coated steel ball to check the friction of coefficient (COF) and wear properties. COF was significantly reduced by 3.3 times compared to Si substrate, and with the addition of graphene by 37%, COF was further reduced by 37.7% compared to pristine MXene. Yang et al. [120] reported 3D MXene carbon nanotube (3D MXene-CNT architecture electrode by gel assembly and chemical vapor deposition method for Li-ion batteries (LIBs) as anode materials. The as-synthesized 3D Mxene-CNT electrode shows a good reversible capacity of 590 mA h g^{-1} at 0.1 A g^{-1} and outstanding rate performance with a capacity of 191 mA h g^{-1} at 5.0 A g^{-1}. The LIB device with 3D Mxene-CNT electrode demonstrates a high energy density of 201 Wh kg^{-1} at a power density of 210 W kg^{-1}, and an excellent energy density of 92 Wh kg^{-1} even at a high-power density of 21 000 W kg^{-1}, as well as good capacity retention of 84.7% after 3500 cycles at 2.0 A g^{-1}. The excellent performance of The LIB device with 3D Mxene-CNT electrode was due to exposure of a high number of Ti atoms on the surface of the MXene, which boosted the redox reaction. Table 3 specifies the various carbon materials synthesized with MXene for different applications.

5 Chalcogenides-Based MXene Composites

MXene 2D materials have many advantages: large specific surface area, large interlayer distance, superior electrical and thermal conductivity. However, layer restacking is one of the major drawbacks of MXene owing to hydrogen bonding or van der Waals forces between the layers which considerably hinder the utilization of MXenes for their full potential. Transition metal chalcogenides and dichalcogenides (TMCs) based nanomaterials such as sulfides (S), selenides (Se), tellurides (Te), MoS_2, WS_2, and $MoSe_2$ have been explored significantly as electrode materials in recent years owing to their excellent specific surface area, atomically thin layered arrangement, superior electrical properties, and stability [129, 130]. These chalcogenide-based nanomaterials can be used to overcome the shortcomings arising from MXene by dispersing uniformly on the surface of each layer of MXene, reducing the restacking of the MXenes and enhancing the electrochemical properties due to their synergistic interaction between MXene and TMCs [131]. Li and co-workers proved that the MXene alone is ineffective for aluminium batteries and also mentioned that conductivity increased significantly with MXene composites doped with cetyltrimethylammonium bromide (CTAB) and selenium. The MXene alone in an aluminium battery initially exhibits the specific capacity of 150 mAh

Table 3 Carbon-based MXene composites

S. no	MXenes	Carbon type	Measuring parameters	Applications	References
1	$Ti_3C_2T_x$	CNTs	130 S/cm conductivity 58 and 187 dB $cm^2\ g^{-1}$	EMI shielding	[121]
2	$Ti_3C_2T_x$	Cellulose	−43.4 dB reflection loss	Microwave absorption and aeronautics	[122]
3	Mixed-$Ti_3C_2T_x$	SWCNT	300 F/cm^3 volumetric capacitance 286 S/cm conductivity	Electrochemical capacitors	[106]
4	Sandwich-like $Ti_3C_2T_x$	SWCNT	390 F/cm^3 volumetric capacitance 385 S/cm conductivity	Electrochemical capacitors	[106]
5	$Ti_3C_2T_x$	CNTs	103.9 dB reflection loss	EMI shielding effect	[123]
6	2D $Ti_3C_2T_x$	Cellulose fiber	35 mg/g desalination capacity	CDI water desalination	[124]
7	Ti_3C_2	Nanodots-interspersed	1957 mAh cm^{-3} volumetric capacity 13.7 mAh cm^{-2} areal capacity	Li–S batteries	[125]
8	Ti_3C_2	CNTs	0.043% fading rate	Li–S cathode	[126]
9	$Ti_3C_2T_x$	CNTs	130% ctretchability 772.6 gauge factor 30–130% sensing range	Sensors	[127]
10	Ti_3C_2	CNTs and cellulose	97.9 ± 5.0 MPa tensile strength 4.6 ± 0.2% fracture strain 2506.6 S/m electrical conductivity and 38.4 dB loss	EMI shielding effect	[128]

g^{-1}. However, after 100 cycles, the specific capacity reduced drastically to 42.8 mAh g^{-1}. MXene composites with CTAB and Selenium (Ti_3C_2@CTAB-Se) showed significant improvement of specific capacity even after 100 cycles. They reported that MXene composites (Ti_3C_2@CTAB-Se) showed a 583.7 mAh g^{-1} specific capacity of 100 mA g^{-1}. Its capacity was still retained to 132.6 mAh g^{-1} even after 400 cycles, showing excellent electrochemical performance of MXene composites (Ti_3C_2@CTAB-Se) compared to pristine MXene. This is due to the reduction of conductivity and stability of MXene, which shows a drastic drop in the specific capacity. However, for MXene composites, specific capacity increased due to increased stability and more active sites, leading to increased electron transfer [132].

Huang et al. [133] synthesized 3D architectures of a few-layered like MXene composites (Ti_3C_2@$NiCo_2Se_4$) anchoring bimetallic nanoparticles of Nickel cobaltous selenide as anode material for SIBs. To fabricate MXene nanosheets, they adopted a novel and a facile solvothermal methodology to support a solution-phase flocculation approach to evade the restacking problem of few-layered Ti_3C_2 MXene nanosheets. In addition, to further stop the self-restacking of MXene nanosheets, they uniformly decorated the zero-dimensional bimetallic selenide $NiCo_2Se_4$, which acts as Na^+ ion reservoir and leads to superior redox activity onto the surface of MXene composite nanosheets and also avoids restacking issues in the MXene sheets as shown in Fig. 10.

The presence of functionalized MXene (f-MXene) nanosheets in f-Ti_3C_2@$NiCo_2Se_4$ composites have a great advantage which endows the composite materials to a rapid electron-Na^+ ion transport capability and, due to the high specific surface of MXene sheets, it enhances the quick charge transfer kinetics and increased interfacial contact between electrolyte–electrode within the battery system. Besides,

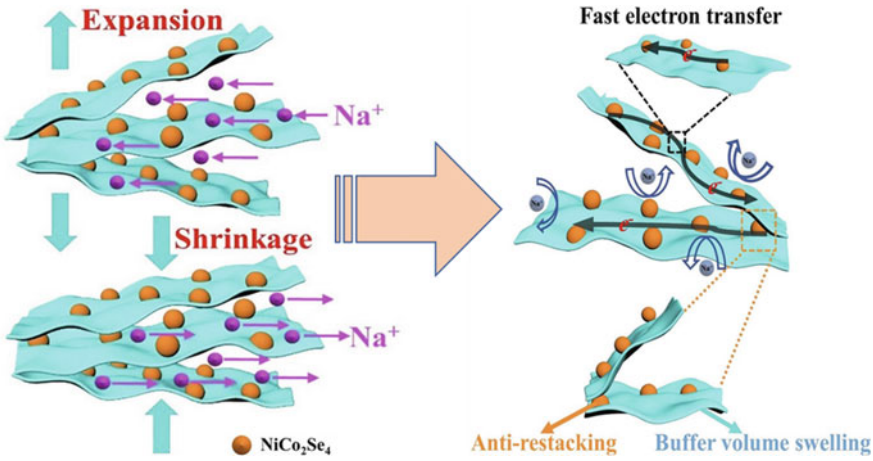

Fig. 10 Schematic representation of expansion and shrinkage abilities and excellent cycling/rate performance mechanism of Ti_3C_2@$NiCo_2Se_4$ composites (reproduced with permission) [133]

as shown in Fig. 11, f-MXene nanosheets were highly flexible to the presence of many surface functional groups that act as a flexible skeleton to dissipate strain caused by $NiCo_2Se_4$ nanoparticles during cycling and restrain pulverization. These excellent properties of MXene nanosheets are responsible for the excellent stability and outstanding electrochemical performance of f-Ti_3C_2@$NiCo_2Se_4$ composites in the sodium-ion battery systems.

Chen and co-workers proposed a novel one-step hydrothermal method to prepare MXene composites with in situ growth of CuSe nanoparticles on the surface of MXene nanosheets. The as-synthesized MXene composites (Ti_3C_2@CuSe) were used as highly efficient counter electrode (CE) material for quantum dot (QD) sensitized solar cells (SCs), showing superior electrical conductivity and polysulfide electrolyte reduction due to their large specific surface area compared to pristine MXene and CuSe nanoparticles [134]. Zong et al. [135] proposed bifunctional electrode materials for lithium storage based on metal–organic frameworks (MOFs) derived CoP anchored MXene composites. They claimed that MXene nanosheets in the MOFs-CoP@MXene/S composites act as a highly stable template for MOFs-CoP, avoiding the enlargement of MOFs-CoP materials on the surface of MXene, yields to exerting its catalytic capability. In addition, since MXene nanosheets have a large number of surface functional groups and high specific surface area, which enhance the possession of LiPS and inhibit the dissolution of polysulfide in the electrolyte. The graphene-like structure of MXene nanosheets exhibits excellent properties such

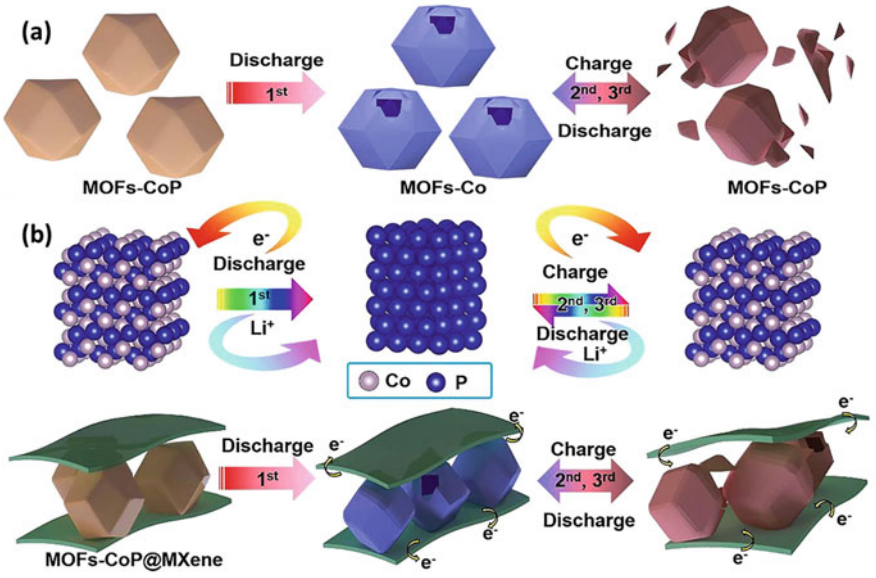

Fig. 11 Schematic representation of MOFs-CoP nanoparticles showing instability (**a**) and their protection and enhanced structural stability under the protection of MXene during cycling (**b**) [135] (reproduced with permission)

as high dimensional stability and superior conductivity within a 3D network of decorating materials on its surface, resulting in excellent electrochemical activities of MXene based composites. The authors demonstrated that MXene composites (MOFs-CoP@MXene/S) as anode material for Li-ion batteries display a high capacity of 706.5 mAh g^{-1} even after 200 cycles at 0.2 A g^{-1}, indicating that MOFs-CoP@MXene/S composites as anode material have robust Li-ion storage capacity. This indicates that it can increase the charge transfer rate and improve Li^+ diffusion kinetics with greater electrochemical activity. The authors proposed a stability mechanism, as shown in Fig. 11. The polyhedral morphology of MOFs-CoP alone showed poor structural stability and got damaged due to charge/discharge cycles since it undergoes large volume changes as an anode material. However, when made composite with Mxene, MXene acted as a substrate to MOFs-CoP nanoparticles and retained their dimensional stability.

Li and co-workers proposed synthesizing MXene nanosheets based composites by combining two or more dichalcogenides which was an effective strategy to exploit their performance as anode materials for Li-ion batteries [136]. They confirmed that SnS_2/Sn_3S_4 dichalcogenides hybrid nanoparticles restricted restacking issues in MXene nanosheets and significantly improved composite's performance. The multilayered Ti_3C_2 MXene nanosheets improved electron mobility, prevented dichalcogenide nanoparticles' agglomeration, and accommodated their volume change during the charge and discharge cycles. They reported that the dichalcogenide based MXene composites showed the best cycling performance (462.3 mAh g^{-1} at 100 mA g^{-1} after 100 cycles) and good rate performance (216.5 mAh g^{-1} at 5000 mA g^{-1}). Recently, Geun Oh and co-workers reported N-doped C-coated $CoSe_2$ incorporated with Ti_3C_2 MXene for electrochemical sodium (Na) and potassium (K) ion storages [137]. $CoSe_2$@NC/MXene attained the reversible capacities of 358 mAh g^{-1} and 317 mAh g^{-1} for potassium and sodium ion storage. In addition, this material achieves the capacitive contribution of 93%, which helps to enhance the kinetic charge transfer performance under the charging and discharging process. Moreover, in Table 4, we also mentioned other chalcogenides materials with MXene and its applications. A ZnCdS/TiO_2/Na-MXene nanocomposites were synthesized by a facile hydrothermal method in which Na^+ and ZnCdS nanoparticles were wrapped by MXene nanosheets [138]. This novel ZnCdS/TiO_2/Na-MXene nanocomposites shows an excellent photocatalyst with a photo-corrosion resistant property. The MXene restacking was minimized due to the intercalation of ZnCdS, which could facilitate the transportation and adsorption of organic pollutants in ZnCdS/TiO_2/Na-MXene nanocomposites. It is evident that the ZnCdS/TiO_2/Na-MXene nanocomposites show an excellent separation competence of electron–hole pairs and outstanding transfer efficiency of electrons on the surface of the MXene nanosheets because of their high electron conductive property.

Table 4 Chalcogenides-based MXenes composites

S. no	MXenes	Chalcogenides	Measuring parameters	Applications	References
1	$Ti_3C_2T_x$	MoS_2	290.7 mAh g^{-1} capacity	K-Ion batteries	[139]
2	$Ti_3C_2T_x$	Co-NiS	911 mAh g^{-1} capacity for Li-Storage 542 mAh g^{-1} capacity for Na-Storage	Li and Na storage batteries	[140]
3	$Ti_3C_2T_x$@C	$MoSe_2$	355 mAh g^{-1} capacity	K-Ion batteries	[141]
4	3D $Ti_3C_2T_x$	N-$CoSe_2$	1084 Wh kg^{-1} energy density	Zn-air batteries	[142]
5	Mo_2CT_x	2H-MoS_2	-450 mA $cm^{-2}{}_{geom}$	Hydrogen evolution reaction (HER) And water splitting application	[143]
6	$Ti_3C_2T_x$	MoS_2	0.39 pg mL^{-1} limit of detection (LOD)	Electrochemical aptasensor	[144]
7	$Ti_3C_2T_x$	MoS_2	-65.51 dB reflection loss	Microwave absorption	[145]
8	$Ti_3C_2T_x$	CdS-MoS_2	9679 μmol.g^{-1} h^{-1} 2.63 ns photoluminescence life time	Photocatalytic H_2 generation	[146]
9	Ti_3C_2	1 T-MoS_2	386.7 F g^{-1} specific capacitance 91.1% retention	Supercapacitors	[147]
10	$Ti_3C_2T_x$	BlueP/MoS_2	203°/RIU sensitivity	Biosensors	[148]

6 Organic Hybrid-MXene Composites

Hybrid composites of two or more materials are always effective for enhancing structural stability and overall performance. Moreover, it is well known that the MXene nanosheets alone are not enough for the required performance in many applications such as batteries, EMI shielding, dielectric materials, etc. Zhang et al. [149] proposed a 3D hybrid composite synthesized by a facile and simple method involving TiO@nitrogen doped carbon/Fe_7S_8 with in situ polymerization of polypyrrole monomer on alkalized MXene for lithium-ion batteries anode material. This MXene hybrid composite (TiO_2@NC/Fe_7S_8) has exceptional architecture where 3D urchin-like TiO_2 with good dimensional stability offers suitable space to improve the contact between electrode–electrolyte. In addition to this, the MXene hybrid composite limits the diffusion rate of lithium-ion and improves the volume change. Nitrogen-doped carbon shell layer increases the electrical conductivity, enables the transportation of electrons, and avoids the accumulation of Fe_7S_8. Fe_7S_8 provides high specific capacity during the charge and discharge process. The MXene composites (TiO_2@NC/Fe_7S_8) showed excellent electrochemical activity such as the reversible capacity of 516 mAh g^{-1} after continuous 100 charge/discharge cycles at 0.1 A g^{-1},

terrific rate capability of 337 mAh g^{-1} at 1 A g^{-1} current density and also a robust long-life span of 282 mAh g^{-1} after the 1000 charge and discharge cycles at 4 A g^{-1}.

Yao et al. [150] made the 3D hierarchical porous hybrid MXene composites derived from CoS based MOF for advanced alkali-ion batteries. The in situ formed MOF structure between the MXene nanosheets can effectively restrict the restacking of nanosheets, as indicated in Fig. 12. This enables the formation of an ordered 3D porous conductive network with a lightweight quality. The hierarchical structure of MOFs@MXene composites is a highly interlocked MXene system with ultra-fine nano-crystallization of the electrochemically active phase of CoS nanoparticles. The hybrid MXene composite system demonstrated excellent electron transport and ions transport properties. Benefiting from the synergistic effect of the individual components, CoS NP@NHC of MXene composite demonstrated exceptional electrochemistry properties as an active electrode material for many battery systems such as the sodium-ion batteries (SIBs), lithium-ion batteries (LIBs), and potassium-ion batteries (PIBs). The hierarchical structure of MOFs@MXene composites displays excellent cyclic life and rate capacities of 420 mAh g^{-1} at 2 A g^{-1} after 650 cycles for SIBs, 1145.9 mAh g^{-1} at 1 A g^{-1} after 800 cycles and 574.1 mAh g^{-1} at 5 A g^{-1} after 1000 cycles for LIBs, and 210 mAh g^{-1} at 2 A g^{-1} after 500 cycles for PIBs.

Polymer-based composites were mainly used for electric insulation and dielectric applications for many years. However, many polymer composites are found to have a low dielectric response with semiconductors. To overcome this issue and increase the dielectric constant, hybrid polymer composites with MXene nanosheets are effective. Deng et al. [151] synthesized special polymer and ceramic doped hybrid vanadium-based MXene composites with excellent dielectric properties. The as-prepared composites showed good dielectric and excellent properties dielectric properties due to strong electron polarization at heterojunction between ceramic and

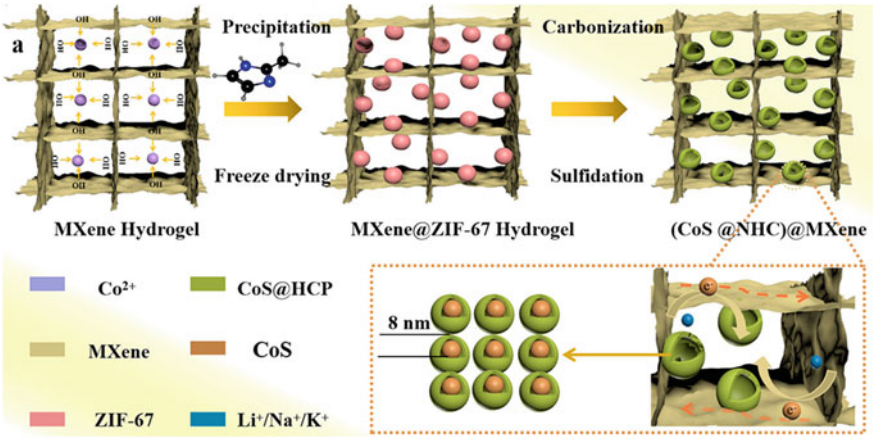

Fig. 12 Schematic representing the synthesis steps of MXene and its hybrid composites with CoS NP@NHC [150] (reproduced with permission)

MXene materials and fluorine-induced electron trap effect. MXene hybrid composites (polymer/V_2C-CuO) demonstrated enhanced electrical properties compared to polymer/Cuo composites. The authors claimed that the hybrid composite with 10 wt% CuO@MXene (V_3C) nanosheets displays a low dielectric loss of 0.23, high dielectric constant of 89, high breakdown strength of 204 MV m^{-1} and low conductivity of 6.8×10^{-7} S m^{-1} at 100 Hz.

Flexible and wearable electronic devices such as artificial electronic skins, motion detection, biomedical monitors and pressure sensors are very common nowadays and important for our day-to-day lives. MXene based hybrid composites are more effective and easy to fabricate with good mechanical stability, high sensitivity, cost-effective and high detection range [152]. Peng et al. [153] introduced highly stable hydrophobic hybrid composites of MXene/rGO/polymer to use pressure sensors for health monitoring. A simple spin-coating method was employed to fabricate MXene composites thin sheet with reduced graphene oxide (rGO) and polymer hybrid materials (PVDF-TrFE). The device displayed a good sensitivity of 2298 k/Pa, less detection limit 8 Pa, and response time of 10 ms, respectively, and it demonstrated excellent stability even after 10,000 cycles. Piezoresistive sensors comprised of Mxene/rGO/P(VDF-TrFE) composite can easily obtain signals less than 8 Pa so that it can test adult pulses randomly. The device's high sensitivity is mainly due to polymer, which acts as an aerogel. When squeezed, the pores were formed to increase the contact area, resulting in an increased current. The authors claimed that the MXene nanosheets in the composite system enhance the sensor's metallic conductivity, leading to an increase in the pressure sensing property. Furthermore, the polymer (P(VDF-TrFE)) in the composite can generate a recoverable 3D network structure, which can promptly deform to form a corresponding signal when receiving pressure and quickly back to the original state after the pressure is removed. The authors further explained that the sensor has exceptional sensitivity due to the high-pressure area because several micropores in the (P(VDF-TrFE)) sample bend only under higher pressure, which results in the higher sensitivity in the greater force region. The Mxene/rGO/P(VDF-TrFE) composite thin film sensor can check the human physiological signals (pulse rate and finger touch) in real-time. Table 5 identifies the organic-based hybrid MXene materials related to its applications and other parameters.

7 Challenges and Prospects

There are various challenges in preparing MXenes and their composites. The first challenge is linked to the synthesis of the MAX phases itself. At present, the preparation process of MAX phase material has not yet reached maturity, and it is still challenging to prepare single-phase MAX phase material that is free from impurities, thermodynamically, and mechanically stable. The Next challenge is the safe synthesis of MXenes, from their precursors (MAX) to the final product (delaminated MXene). Generally, the majority of MXene is synthesized using HF-based etching

Table 5 Organic hybrid based MXenes composite

S. no	MXenes	Organic hybrid	Measuring parameters	Applications	References
1	Nb_2CT_x	Bi_2WO_6	99.8%, 92.7% and 83.1% Photodegradation efficiency for Rhb, MB and TC-HCl	Photocatalytic activity	[154]
2	$Ti_3C_2T_x$	Quinone-coupled viologen and pyridiniumium derivatives	−2.77 eV binding energy	Pseudocapacitive interaction	[155]
3	$Ti_3C_2T_x$	NiCoOOH-NiCoS	58.2 mV dec^{-1} tafel slope 7.9 nm d_{pore}	Electrocatalytic oxygen evolution Zinc-air batteries	[156]
4	$Ti_3C_2T_x$	Ni chain/ZnO	−35.1 dB reflection loss	Microwave absorption	[157]
5	$Ti_3C_2T_x$	Phenothiazine@RGO	77% Retention 17.4 Wh/Kg energy density	Supercapacitors	[158]
6	Ti_3C_2	Bi_2WO_6	72.8 charge density 85.3 $\mu mol.g^{-1}$ h^{-1}	Photodegradation	[159]
7	$Ti_3C_2T_x$	Polytetrafluoroethylene and CuO	Vg/Va = 24.8 @ 100 ppm 810 V open-circuit voltage 34 μA short-circuit current	Sensors	[160]
8	Ti_3C_2	Ni-Co@NiCo-MOF/NF	2137.5 F g^{-1} specific capacitance 75.3% retention	Hybrid supercapacitors	[161]
9	Ti_3C_2	NH_2-MIL-125(Ti)(TiO_2)	0.9494 ns fluorescence life time 0.034 min^{-1} rate constant	Photocatalytic activity	[162]
10	Ti_3C_2	/CNHs/β-CD-MOFs	3.0 nM to 10.0 μM linear range 1.0 nM (S/N = 3) limit of detection (LOD)	Electrochemical sensing	[163]

approaches, and safe handling and waste treatment are necessary for the HF-based etchant. The next challenge relates to fewer applications of MXene in polymer and organic hybrid composites due to material compatibility and dispersion issues. The majority of applications are related to the dielectric, electrical, mechanical, and EMI shielding performance. Therefore, to derive the full potential of MXene, it is necessary to exploit MXene and its related composites in various other fields like energy, construction, automotive, etc. In addition, more research needs to be directed to the products catering to industrial and commercial needs.

8 Conclusion

This chapter summarises MXenes and their composites and then addresses their performance, fabrication, and applications. The importance of MXenes fabrication with various composites is the main theme of this chapter. Updated information of MXene and composites, namely MXene/metal oxide, MXene/polymer, MXene/carbon, MXene/chalcogenides, and MXene/organic hybrid along with their relevant applications, are highlighted in detail. Due to the large functional group and surface chemistry, MXene/composite has shown many fascinating properties owing to their unique characteristics such as conductivity, biocompatibility, cost-effectiveness, and excellent interlayer spacing. These are the keys behind the enormous attraction of MXenes and their composites. It is worth highlighting that the synthesis routes, surface characterisation, and properties of MXene/composites play a vital role in the performance of 2D materials to employ them as a newly efficient, cost-effective, and excellent friendly environment for the future generation.

References

1. Mas-Ballesté, R., et al.: 2D materials: to graphene and beyond. Nanoscale **3**(1), 20–30 (2011)
2. Novoselov, K.S., et al.: Electric field effect in atomically thin carbon films. Science **306**(5696), 666–669 (2004)
3. Oughaddou, H., et al.: Silicene, a promising new 2D material. Prog. Surf. Sci. **90**(1), 46–83 (2015)
4. Mannix, A.J., et al.: Synthesis and chemistry of elemental 2D materials. Nat. Rev. Chem. **1**(2), 0014 (2017)
5. Kalantar-zadeh, K., et al.: Two dimensional and layered transition metal oxides. Appl. Mater. Today **5**, 73–89 (2016)
6. Naguib, M., et al.: Two-dimensional nanocrystals produced by exfoliation of Ti_3AlC_2. Adv. Mater. **23**(37), 4248–4253 (2011)
7. Zhan, X., et al.: MXene and MXene-based composites: synthesis, properties and environment-related applications. Nanoscale Horiz. **5**(2), 235–258 (2020)
8. Berdiyorov, G.R., Mahmoud, K.A.: Effect of surface termination on Ion intercalation selectivity of bilayer $Ti_3C_2T_2$ (T = F, O and OH) MXene. Appl. Surf. Sci. **416**, 725–730 (2017)
9. Liang, X., Garsuch, A., Nazar, L.F.: Sulfur cathodes based on conductive MXene nanosheets for high-performance lithium-sulfur batteries. Angew. Chem. Int. Ed. **54**(13), 3907–3911 (2015)
10. Mashtalir, O., et al.: Amine-assisted delamination of Nb_2C MXene for Li-Ion energy storage devices. Adv. Mater. **27**(23), 3501–3506 (2015)
11. Xie, X., et al.: Porous heterostructured MXene/carbon nanotube composite paper with high volumetric capacity for sodium-based energy storage devices. Nano Energy **26**, 513–523 (2016)
12. Valden, M., Lai, X., Goodman, D.W.: Onset of catalytic activity of gold clusters on titania with the appearance of nonmetallic properties. Science **281**(5383), 1647–1650 (1998)
13. Rodriguez, J., Dvorak, J., Maiti, A., et al.: J. Am. Chem. Soc. **124**, 5247 (2002)
14. Bäumer, M., Freund, H.-J.: Metal deposits on well-ordered oxide films. Prog. Surf. Sci. **61**(7–8), 127–198 (1999)

15. Trudeau, M., Ying, J.: Nanocrystalline materials in catalysis and electrocatalysis: structure tailoring and surface reactivity. Nanostruct. Mater. **7**(1–2), 245–258 (1996)
16. Ayyub, P., et al.: Effect of crystal size reduction on lattice symmetry and cooperative properties. Phys. Rev. B **51**(9), 6135 (1995)
17. Zhang, H., Banfield, J.F.: Thermodynamic analysis of phase stability of nanocrystalline titania. J. Mater. Chem. **8**(9), 2073–2076 (1998)
18. Nabavi, M., Sanchez, C., Livage, J.: Structure and properties of amorphous V_2O_5. Philos. Mag. B **63**(4), 941–953 (1991)
19. Samsonov, V., Sdobnyakov, N.Y., Bazulev, A.: On thermodynamic stability conditions for nanosized particles. Surf. Sci. **532**, 526–530 (2003)
20. Ayyub, P., et al.: Size-induced structural phase transitions and hyperfine properties of microcrystalline Fe_2O_3. J. Phys. C Solid State Phys. **21**(11), 2229 (1988)
21. Hernández-Alonso, M.D., et al.: Confinement effects in quasi-stoichiometric CeO_2 nanoparticles. Phys. Chem. Chem. Phys. **6**(13), 3524–3529 (2004)
22. Skandan, G., et al.: Phase characterization and stabilization due to grain size effects of nanostructured Y_2O_3. Nanostruct. Mater. **1**(4), 313–322 (1992)
23. Cammarata, R., Sieradzki, K.: Effects of surface stress on the elastic moduli of thin films and superlattices. Phys. Rev. Lett. **62**(17), 2005 (1989)
24. Landfester, K.: Miniemulsion polymerization and the structure of polymer and hybrid nanoparticles. Angew. Chem. Int. Ed. **48**(25), 4488–4507 (2009)
25. Amancio-Filho, S., Dos Santos, J.: Joining of polymers and polymer–metal hybrid structures: recent developments and trends. Polym. Eng. Sci. **49**(8), 1461–1476 (2009)
26. Ovsianikov, A., et al.: Two photon polymerization of polymer–ceramic hybrid materials for transdermal drug delivery. Int. J. Appl. Ceram. Technol. **4**(1), 22–29 (2007)
27. Kickelbick, G.: Hybrid Materials: Synthesis, Characterization, and Applications. Wiley & Sons (2007)
28. Kickelbick, G.: Hybrid Materials-Past, Present and Future (2014)
29. Kickelbick, G.: Introduction to hybrid materials. Hybrid Mater. **1**, 2 (2007)
30. Pyun, J., Matyjaszewski, K.: The synthesis of hybrid polymers using atom transfer radical polymerization: homopolymers and block copolymers from polyhedral oligomeric silsesquioxane monomers. Macromolecules **33**(1), 217–220 (2000)
31. Irfan, M.: Chemistry of polymers. In: Chemistry and Technology of Thermosetting Polymers in Construction Applications, pp. 8–77. Springer (1998)
32. Beachell, H.C., Son, C.N.: Color formation in polyurethanes. J. Appl. Polym. Sci. **7**(6), 2217–2237 (1963)
33. Yu, B., et al.: Interface decoration of exfoliated MXene ultra-thin nanosheets for fire and smoke suppressions of thermoplastic polyurethane elastomer. J. Hazard. Mater. **374**, 110–119 (2019)
34. Beachell, H.C., Son, C.N.: Stabilization of polyurethane to thermal degradation. J. Appl. Polym. Sci. **8**(3), 1089–1096 (1964)
35. Boota, M., et al.: Interaction of polar and nonpolar polyfluorenes with layers of two-dimensional titanium carbide (MXene): intercalation and pseudocapacitance. Chem. Mater. **29**(7), 2731–2738 (2017)
36. Kagan, C.R., Mitzi, D.B., Dimitrakopoulos, C.D.: Organic-inorganic hybrid materials as semiconducting channels in thin-film field-effect transistors. Science **286**(5441), 945–947 (1999)
37. Glavin, N.R., et al.: Emerging applications of elemental 2D materials. Adv. Mater. **32**(7), 1904302 (2020)
38. Lin, Z., et al.: 2D materials advances: from large scale synthesis and controlled heterostructures to improved characterization techniques, defects and applications. 2D Mater. **3**(4), 042001 (2016)
39. Jayakumar, A., Surendranath, A., Mohanan, P.: 2D materials for next generation healthcare applications. Int. J. Pharm. **551**(1–2), 309–321 (2018)

40. Luo, B., Liu, G., Wang, L.: Recent advances in 2D materials for photocatalysis. Nanoscale **8**(13), 6904–6920 (2016)
41. Shi, L., Zhao, T.: Recent advances in inorganic 2D materials and their applications in lithium and sodium batteries. J. Mater. Chem. A **5**(8), 3735–3758 (2017)
42. Yu, S., et al.: 2D materials for optical modulation: challenges and opportunities. Adv. Mater. **29**(14), 1606128 (2017)
43. Han, Y., et al.: Recent progress in 2D materials for flexible supercapacitors. J. Energy Chem. **27**(1), 57–72 (2018)
44. Li, Y., et al.: V_2O_5 nanopaper as a cathode material with high capacity and long cycle life for rechargeable aqueous zinc-ion battery. Nano Energy **60**, 752–759 (2019)
45. Li, J., et al.: K-Ion storage enhancement in Sb_2O_3/reduced graphene oxide using ether-based electrolyte. Adv. Energy Mater. **10**(5), 1903455 (2020)
46. Xu, G., et al.: Three-dimensional hydrated vanadium pentoxide/MXene composite for high-rate zinc-ion batteries. J. Colloid Interface Sci. **593**, 417–423 (2021)
47. Song, C., et al.: Enhanced polysulfide conversion through metal oxide-support interaction in MnOx/MXene. Chem. Eng. J. **420**, 130452 (2021)
48. Long, C., et al.: High-performance asymmetric supercapacitors with lithium intercalation reaction using metal oxide-based composites as electrode materials. J. Mater. Chem. A **2**(39), 16678–16686 (2014)
49. Wu, W., et al.: Ultrathin N-doped Ti_3C_2-MXene decorated with $NiCo_2S_4$ nanosheets as advanced electrodes for supercapacitors. Appl. Surf. Sci. **539**, 148272 (2021)
50. Huang, J., et al.: Sandwich-like Na0.23TiO_2 nanobelt/Ti_3C_2 MXene composites from a scalable in situ transformation reaction for long-life high-rate lithium/sodium-ion batteries. Nano Energy **46**, 20–28 (2018)
51. Yin, J., et al.: Self-assembled sandwich-like MXene-derived composites as highly efficient and sustainable catalysts for wastewater treatment. Langmuir **37**(3), 1267–1278 (2021)
52. Hou, T., et al.: MXene-based accordion 2D hybrid structure with Co_9S_8/C/$Ti_3C_2T_x$ as efficient electromagnetic wave absorber. Chem. Eng. J. **414**, 128875 (2021)
53. Liu, M., et al.: In_2O_3 nanocubes/Ti_3C_2Tx MXene composites for enhanced methanol gas sensing properties at room temperature. Ceram. Int. (2021)
54. Zhang, X., et al.: Improved electrochemical performance of CoOx-NiO/$Ti_3C_2T_x$ MXene nanocomposites by atomic layer deposition towards high capacitance supercapacitors. J. Alloy Compd. **862**, 158546 (2021)
55. Liu, M., et al.: Flexible MXene/rGO/CuO hybrid aerogels for high performance acetone sensing at room temperature. Sens. Actuators B Chem. **340**, 129946 (2021)
56. Zhu, K., et al.: Two-dimensional titanium carbide MXene as a capacitor-type electrode for rechargeable aqueous Li-Ion and Na-Ion capacitor batteries. ChemElectroChem **4**(11), 3018–3025 (2017)
57. Su, T., et al.: Monolayer $Ti_3C_2T_x$ as an effective co-catalyst for enhanced photocatalytic hydrogen production over TiO_2. ACS Appl. Energy Mater. **2**(7), 4640–4651 (2019)
58. Zheng, W., et al.: Microwave-assisted synthesis of SnO_2-Ti_3C_2 nanocomposite for enhanced supercapacitive performance. Mater. Lett. **209**, 122–125 (2017)
59. Gao, Y., et al.: Hydrothermal synthesis of TiO_2/Ti_3C_2 nanocomposites with enhanced photocatalytic activity. Mater. Lett. **150**, 62–64 (2015)
60. Rakhi, R.B., et al.: Direct chemical synthesis of MnO_2 nanowhiskers on transition-metal carbide surfaces for supercapacitor applications. ACS Appl. Mater. Interfaces **8**(29), 18806–18814 (2016)
61. Zhang, Z., et al.: Highly-dispersed iron oxide nanoparticles anchored on crumpled nitrogen-doped MXene nanosheets as anode for Li-ion batteries with enhanced cyclic and rate performance. J. Power Sources **439**, 227107 (2019)
62. Wang, Z., et al.: Photo-synergetic nitrogen-doped MXene/reduced graphene oxide sandwich-like architecture for high-performance lithium-sulfur batteries. Int. J. Energy Res. **45**(2), 2728–2738 (2021)

63. Zhao, S., et al.: Highly electrically conductive three-dimensional $Ti_3C_2T_x$ MXene/reduced graphene oxide hybrid aerogels with excellent electromagnetic interference shielding performances. ACS Nano **12**(11), 11193–11202 (2018)
64. Sudheer, V., SarathKumar, S., Sankararaman, S.: Nanostructured ZnO and ZnO: Pd with MXene overlayer SPR biosensors. Opt. Quant. Electron. **53**(6), 1–14 (2021)
65. Cao, J., et al.: Alternative electrodes for HTMs and noble-metal-free perovskite solar cells: 2D MXenes electrodes. RSC Adv. **9**(59), 34152–34157 (2019)
66. Lin, Q., et al.: Self-cleaning photocatalytic MXene composite membrane for synergistically enhanced water treatment: oil/water separation and dyes removal. Chem. Eng. J. **427**, 131668 (2022)
67. Tahir, T., et al.: Synthesis of sponge like Gd3+ doped vanadium oxide/2D MXene composites for improved degradation of industrial effluents and pathogens. Ceram. Int. **48**(2), 1969–1980 (2022)
68. Ji, C., et al.: Ice-templated MXene/Ag–epoxy nanocomposites as high-performance thermal management materials. ACS Appl. Mater. Interfaces **12**(21), 24298–24307 (2020)
69. Novoselov, K.S., et al.: A roadmap for graphene. Nature **490**(7419), 192–200 (2012)
70. Geim, A.K., Novoselov, K.S.: The rise of graphene. In: Nanoscience and Technology: A Collection of Reviews From Nature Journals, pp. 11–19. World Scientific (2010)
71. Zhang, Z., et al.: Mechanically strong MXene/Kevlar nanofiber composite membranes as high-performance nanofluidic osmotic power generators. Nat. Commun. **10**(1), 1–9 (2019)
72. Sun, Y., et al.: MXene-xanthan nanocomposite films with layered microstructure for electromagnetic interference shielding and Joule heating. Chem. Eng. J. **410**, 128348 (2021)
73. Yang, H., et al.: Layered PVB/$Ba_3Co_2Fe_{24}O_{41}$/Ti_3C_2 Mxene composite: enhanced electromagnetic wave absorption properties with high impedance match in a wide frequency range. Mater. Chem. Phys. **200**, 179–186 (2017)
74. Jiang, C., et al.: All-electrospun flexible triboelectric nanogenerator based on metallic MXene nanosheets. Nano Energy **59**, 268–276 (2019)
75. Shao, W., et al.: Polyester@MXene nanofibers-based yarn electrodes. J. Power Sources **396**, 683–690 (2018)
76. Xu, H., et al.: Lightweight Ti_2CT_x MXene/Poly(vinyl alcohol) composite foams for electromagnetic wave shielding with absorption-dominated feature. ACS Appl. Mater. Interfaces **11**(10), 10198–10207 (2019)
77. Zhou, Z., et al.: Layer-by-layer assembly of MXene and carbon nanotubes on electrospun polymer films for flexible energy storage. Nanoscale **10**(13), 6005–6013 (2018)
78. Zhang, C., et al.: Two-dimensional transition metal carbides and nitrides (MXenes): synthesis, properties, and electrochemical energy storage applications. Energy & Environ. Mater. **3**(1), 29–55 (2020)
79. Wang, J., et al.: A new strategy for high-performance electromagnetic interference shielding by designing a layered double-percolated structure in PS/PVDF/MXene composites. Eur. Polymer J. **151**, 110450 (2021)
80. Jin, X., et al.: Flame-retardant poly(vinyl alcohol)/MXene multilayered films with outstanding electromagnetic interference shielding and thermal conductive performances. Chem. Eng. J. **380**, 122475 (2020)
81. Liu, F., et al.: Well-aligned MXene/chitosan films with humidity response for high-performance electromagnetic interference shielding. Carbohyd. Polym. **243**, 116467 (2020)
82. Shi, Y., et al.: Strengthening, toughing and thermally stable ultra-thin MXene nanosheets/polypropylene nanocomposites via nanoconfinement. Chem. Eng. J. **378**, 122267 (2019)
83. Xu, M.-K., et al.: Electrically Conductive $Ti_3C_2T_x$ MXene/polypropylene nanocomposites with an ultralow percolation threshold for efficient electromagnetic interference shielding. Ind. Eng. Chem. Res. **60**(11), 4342–4350 (2021)
84. Xue, Y., et al.: Polyphosphoramide-intercalated MXene for simultaneously enhancing thermal stability, flame retardancy and mechanical properties of polylactide. Chem. Eng. J. **397**, 125336 (2020)

85. Luo, J.-Q., et al.: Flexible, stretchable and electrically conductive MXene/natural rubber nanocomposite films for efficient electromagnetic interference shielding. Compos. Sci. Technol. **182**, 107754 (2019)
86. Hatter, C.B., et al.: Micromechanical response of two-dimensional transition metal carbonitride (MXene) reinforced epoxy composites. Compos. B Eng. **182**, 107603 (2020)
87. Pan, Y., et al.: Flammability, thermal stability and mechanical properties of polyvinyl alcohol nanocomposites reinforced with delaminated $Ti_3C_2T_x$ (MXene). Polym. Compos. **41**(1), 210–218 (2020)
88. Zhao, L., et al.: Highly-stable polymer-crosslinked 2D MXene-based flexible biocompatible electronic skins for in vivo biomonitoring. Nano Energy **84**, 105921 (2021)
89. Zhou, Z., et al.: Facile fabrication of densely packed Ti_3C_2 MXene/nanocellulose composite films for enhancing electromagnetic interference shielding and electro-/photothermal performance. ACS Nano **15**(7), 12405–12417 (2021)
90. McDaniel, R.M., et al.: Well-dispersed nanocomposites using covalently modified, multilayer, 2D titanium carbide (MXene) and in-situ "Click" polymerization. Chem. Mater. **33**(5), 1648–1656 (2021)
91. Zheng, Y., et al.: High conductivity and stability of polystyrene/MXene composites with orientation-3D network binary structure. J. Colloid Interface Sci. **595**, 151–158 (2021)
92. Mao, Y., Wang, D., Fu, S.: Layer-by-layer self-assembled nanocoatings of Mxene and P, N-co-doped cellulose nanocrystals onto cotton fabrics for significantly reducing fire hazards and shielding electromagnetic interference. Compos. A Appl. Sci. Manuf. **153**, 106751 (2022)
93. Qin, L., et al.: Polymer-MXene composite films formed by MXene-facilitated electrochemical polymerization for flexible solid-state microsupercapacitors. Nano Energy **60**, 734–742 (2019)
94. Jin, X., et al.: Flame-retardant poly (vinyl alcohol)/MXene multilayered films with outstanding electromagnetic interference shielding and thermal conductive performances. Chem. Eng. J. **380**, 122475 (2020)
95. Mazhar, S., et al.: Promising PVC/MXene based flexible thin film nanocomposites with excellent dielectric, thermal and mechanical properties. Ceram. Int. **46**(8), 12593–12605 (2020)
96. Ren, Y., et al.: Synthesis of polyaniline nanoparticles deposited on two-dimensional titanium carbide for high-performance supercapacitors. Mater. Lett. **214**, 84–87 (2018)
97. Zhang, J., et al.: MXene: a potential candidate for yarn supercapacitors. Nanoscale **9**(47), 18604–18608 (2017)
98. Yu, L., et al.: $Ti_3C_2T_x$ (MXene)-silicon heterojunction for efficient photovoltaic cells. Adv. Energy Mater. **9**(31), 1901063 (2019)
99. Wei, H., et al.: $Ti_3C_2T_x$ MXene/polyaniline (PANI) sandwich intercalation structure composites constructed for microwave absorption. Compos. Sci. Technol. **169**, 52–59 (2019)
100. Sheng, X., et al.: Properties of two-dimensional Ti_3C_2 MXene/thermoplastic polyurethane nanocomposites with effective reinforcement via melt blending. Compos. Sci. Technol. **181**, 107710 (2019)
101. Ling, Z., et al.: Flexible and conductive MXene films and nanocomposites with high capacitance. Proc. Natl. Acad. Sci. **111**(47), 16676–16681 (2014)
102. Karousis, N., et al.: Structure, properties, functionalization, and applications of carbon nanohorns. Chem. Rev. **116**(8), 4850–4883 (2016)
103. Rao, R., et al.: Carbon nanotubes and related nanomaterials: critical advances and challenges for synthesis toward mainstream commercial applications. ACS Nano **12**(12), 11756–11784 (2018)
104. Olabi, A.G., et al.: application of graphene in energy storage device—a review. Renew. Sustain. Energy Rev. **135**, 110026 (2021)
105. Sun, L., et al.: MXene/N-doped carbon foam with three-dimensional hollow neuron-like architecture for freestanding, highly compressible all solid-state supercapacitors. ACS Appl. Mater. Interfaces **12**(40), 44777–44788 (2020)
106. Zhao, M.-Q., et al.: Flexible MXene/carbon nanotube composite paper with high volumetric capacitance. Adv. Mater. **27**(2), 339–345 (2015)

107. Zhou, S., et al.: Heterostructures of MXenes and N-doped graphene as highly active bifunctional electrocatalysts. Nanoscale **10**(23), 10876–10883 (2018)
108. Dwivedi, N., et al.: Emergent 2D materials for combating infectious diseases: the potential of MXenes and MXene–graphene composites to fight against pandemics. Mater. Adv. **2**(9), 2892–2905 (2021)
109. Liu, Y., et al.: graphene enhanced flexible expanded graphite film with high electric, thermal conductivities and EMI shielding at low content. Carbon **133**, 435–445 (2018)
110. Wan, L., et al.: construction of two-dimensional bimetal (Fe-Ti) oxide/carbon/MXene architecture from titanium carbide MXene for ultrahigh-rate lithium-ion storage. J. Colloid Interface Sci. **588**, 147–156 (2021)
111. Liu, Y., et al.: Highly thermal conductivity and flame retardant flexible graphene/MXene paper based on an optimized interface and nacre laminated structure. Compos. A Appl. Sci. Manuf. **141**, 106227 (2021)
112. Qi, F., et al.: Robust $Ti_3C_2T_x$ MXene/starch derived carbon foam composites for superior EMI shielding and thermal insulation. Mater. Today Phys. **21**, 100512 (2021)
113. Aïssa, B., et al.: Nanoelectromagnetic of a highly conductive 2D transition metal carbide (MXene)/graphene nanoplatelets composite in the EHF M-band frequency. Carbon **173**, 528–539 (2021)
114. Rasheed, A.K., et al.: graphene based nanofluids and nanolubricants—review of recent developments. Renew. Sustain. Energy Rev. **63**, 346–362 (2016)
115. Kinoshita, H., et al.: Tribological properties of monolayer graphene oxide sheets as water-based lubricant additives. Carbon **66**, 720–723 (2014)
116. Rosenkranz, A., et al.: Multi-layer $Ti_3C_2T_x$-nanoparticles (MXenes) as solid lubricants—role of surface terminations and intercalated water. Appl. Surf. Sci. **494**, 13–21 (2019)
117. Zhao, X., et al.: pH, nanosheet concentration, and antioxidant affect the oxidation of $Ti_3C_2T_x$ and Ti_2CT_x MXene dispersions. Adv. Mater. Interfaces **7**(20), 2000845 (2020)
118. Huang, S., et al.: Achieving superlubricity with 2D transition metal carbides (MXenes) and MXene/graphene coatings. Mater. Today Adv. **9**, 100133 (2021)
119. Lian, W., et al.: Ti_3C_2/graphene oxide heterostructural coating with enhanced dry tribological performance. Appl. Nanosci. **11**(5), 1471–1479 (2021)
120. Yang, B., et al.: Realizing high-performance lithium ion hybrid capacitor with a 3D MXene-carbon nanotube composite anode. Chem. Eng. J. **429**, 132392 (2022)
121. Weng, G.M., et al.: Layer-by-layer assembly of cross-functional semi-transparent MXene-carbon nanotubes composite films for next-generation electromagnetic interference shielding. Adv. Func. Mater. **28**(44), 1803360 (2018)
122. Jiang, Y., et al.: Hierarchically structured cellulose aerogels with interconnected MXene networks and their enhanced microwave absorption properties. J. Mater. Chem. C **6**(32), 8679–8687 (2018)
123. Sambyal, P., et al.: Ultralight and mechanically robust $Ti_3C_2T_x$ hybrid aerogel reinforced by carbon nanotubes for electromagnetic interference shielding. ACS Appl. Mater. Interfaces **11**(41), 38046–38054 (2019)
124. Anwer, S., et al.: 2D $Ti_3C_2T_x$ MXene nanosheets coated cellulose fibers based 3D nanostructures for efficient water desalination. Chem. Eng. J. **406**, 126827 (2021)
125. Xiao, Z., et al.: Ultrafine Ti_3C_2 MXene nanodots-interspersed nanosheet for high-energy-density lithium–sulfur batteries. ACS Nano **13**(3), 3608–3617 (2019)
126. Liang, X., et al.: Interwoven MXene nanosheet/carbon-nanotube composites as Li–S cathode hosts. Adv. Mater. **29**(3), 1603040 (2017)
127. Cai, Y., et al.: Stretchable $Ti_3C_2T_x$ MXene/carbon nanotube composite based strain sensor with ultrahigh sensitivity and tunable sensing range. ACS Nano **12**(1), 56–62 (2018)
128. Cao, W., et al.: Ultrathin and flexible CNTs/MXene/cellulose nanofibrils composite paper for electromagnetic interference shielding. Nano-Micro Lett. **11**(1), 1–17 (2019)
129. Gao, M.-R., et al.: Nanostructured metal chalcogenides: synthesis, modification, and applications in energy conversion and storage devices. Chem. Soc. Rev. **42**(7), 2986–3017 (2013)

130. Choi, W., et al.: Recent development of two-dimensional transition metal dichalcogenides and their applications. Mater. Today **20**(3), 116–130 (2017)
131. Zhang, F., et al.: Interface engineering of MXene composite separator for high-performance Li–Se and Na–Se batteries. Adv. Energy Mater. **10**(20), 2000446 (2020)
132. Li, Z., et al.: Two-dimensional Ti_3C_2@CTAB-Se (MXene) composite cathode material for high-performance rechargeable aluminum batteries. Chem. Eng. J. **398**, 125679 (2020)
133. Huang, P., et al.: Few-layered Ti_3C_2 MXene anchoring bimetallic selenide $NiCo_2Se_4$ nanoparticles for superior Sodium-ion batteries. Chem. Eng. J. **417**, 129161 (2021)
134. Chen, Y., et al.: In suit growth of CuSe nanoparticles on MXene (Ti_3C_2) nanosheets as an efficient counter electrode for quantum dot-sensitized solar cells. Electrochim. Acta **316**, 248–256 (2019)
135. Zong, H., et al.: Metal-organic frameworks-derived CoP anchored on MXene toward an efficient bifunctional electrode with enhanced lithium storage. Chem. Eng. J. **416**, 129102 (2021)
136. Li, J., et al.: MXene-decorated SnS_2/Sn_3S_4 hybrid as anode material for high-rate lithium-ion batteries. Chem. Eng. J. **380**, 122590 (2020)
137. Oh, H.G., et al.: N-doped carbon-coated $CoSe_2$ nanocrystals anchored on two-dimensional MXene nanosheets for efficient electrochemical sodium-and potassium-ion storage. Int. J. Energy Res. **45**(12), 17738–17748 (2021)
138. Qin, X., et al.: Hydrothermal growth of ZnCdS/TiO_2 nanoparticles on the surface of the Ti_3C_2 MXene sheet to enhance photocatalytic performance under visible light. J. Solid State Chem. **306**, 122750 (2022)
139. Li, J., et al.: Nanosheets assembled layered MoS_2/MXene as high performance anode materials for potassium ion batteries. J. Power Sources **449**, 227481 (2020)
140. Zou, Z., et al.: Versatile interfacial self-assembly of $Ti_3C_2T_x$ MXene based composites with enhanced kinetics for superior lithium and sodium storage. ACS Nano **15**(7), 12140–12150 (2021)
141. Huang, H., et al.: Carbon-coated $MoSe_2$/MXene hybrid nanosheets for superior potassium storage. ACS Nano **13**(3), 3448–3456 (2019)
142. Zeng, Z., et al.: Bifunctional N-$CoSe_2$/3D-MXene as highly efficient and durable cathode for rechargeable Zn–air battery. ACS Mater. Lett. **1**(4), 432–439 (2019)
143. Lim, K.R.G., et al.: 2h-Mos_2 on Mo_2CT_x Mxene nanohybrid for efficient and durable electrocatalytic hydrogen evolution. ACS Nano **14**(11), 16140–16155 (2020)
144. Kashefi-Kheyrabadi, L., et al.: A MoS_2@ $Ti_3C_2T_x$ MXene hybrid-based electrochemical aptasensor (MEA) for sensitive and rapid detection of thyroxine. Bioelectrochemistry **137**, 107674 (2021)
145. Wang, J., et al.: Hierarchical carbon fiber@ MXene@ MoS_2 core-sheath synergistic microstructure for tunable and efficient microwave absorption. Adv. Func. Mater. **30**(45), 2002595 (2020)
146. Chen, R., et al.: Synergetic effect of MoS_2 and MXene on the enhanced H_2 evolution performance of CdS under visible light irradiation. Appl. Surf. Sci. **473**, 11–19 (2019)
147. Wang, X., et al.: 2D/2D 1T-MoS_2/Ti_3C_2 MXene heterostructure with excellent supercapacitor performance. Adv. Func. Mater. **30**(15), 0190302 (2020)
148. Pal, S., et al.: Sensitivity analysis of surface plasmon resonance biosensor based on heterostructure of 2D BlueP/MoS_2 and MXene. Layer. 2D Adv. Mater. Their Allied Appl. 103–129 (2020)
149. Zhang, X., et al.: 3D TiO_2@nitrogen-doped carbon/Fe_7S_8 composite derived from polypyrrole-encapsulated alkalized MXene as anode material for high-performance lithium-ion batteries. Chem. Eng. J. **385**, 123394 (2020)
150. Yao, L., Gu, Q., Yu, X.: Three-Dimensional MOFs@MXene aerogel composite derived MXene threaded hollow carbon confined CoS nanoparticles toward advanced Alkali-Ion batteries. ACS Nano **15**(2), 3228–3240 (2021)
151. Deng, Q., et al.: Remarkably improving dielectric response of polymer/hybrid ceramic composites based on 0D/2D-stacked CuO/V2C MXene heterojunction. Appl. Surf. Sci. **545**, 149008 (2021)

152. Pei, Y., et al.: $Ti_3C_2T_x$ MXene for sensing applications: recent progress, design principles, and future perspectives. ACS Nano **15**(3), 3996–4017 (2021)
153. Peng, Z., et al.: Hydrophobic and stable MXene/reduced graphene oxide/polymer hybrid materials pressure sensors with an ultrahigh sensitive and rapid response speed pressure sensor for health monitoring. Mater. Chem. Phys. 124729 (2021)
154. Cui, C., et al.: Bi_2WO_6/Nb_2CT_x MXene hybrid nanosheets with enhanced visible-light-driven photocatalytic activity for organic pollutants degradation. Appl. Surf. Sci. **505**, 144595 (2020)
155. Boota, M., et al.: Mechanistic understanding of the interactions and pseudocapacitance of multi-electron redox organic molecules sandwiched between MXene layers. Adv. Electron. Mater. **7**(4), 2001202 (2021)
156. Zou, H., et al.: Metal–organic framework-derived nickel–cobalt sulfide on ultrathin mxene nanosheets for electrocatalytic oxygen evolution. ACS Appl. Mater. Interfaces **10**(26), 22311–22319 (2018)
157. Wang, S., et al.: Hierarchical $Ti_3C_2T_x$ MXene/Ni Chain/ZnO array hybrid nanostructures on cotton fabric for durable self-cleaning and enhanced microwave absorption. ACS Nano **14**(7), 8634–8645 (2020)
158. Boota, M., Bécuwe, M., Gogotsi, Y.: Phenothiazine–MXene aqueous asymmetric pseudocapacitors. ACS Appl Energy Mater **3**(4), 3144–3149 (2020)
159. Huang, G., et al.: Ti_3C_2 MXene-modified Bi_2WO_6 nanoplates for efficient photodegradation of volatile organic compounds. Appl. Surf. Sci. **503**, 144183 (2020)
160. Wang, D., et al.: Multifunctional latex/polytetrafluoroethylene-based triboelectric nanogenerator for self-powered organ-like MXene/Metal–organic framework-derived CuO nanohybrid ammonia sensor. ACS Nano **15**(2), 2911–2919 (2021)
161. Wang, J., et al.: Construction of hexagonal nickel-cobalt oxide nanosheets on metal-organic frameworks based on MXene interlayer ion effect for hybrid supercapacitors. J. Alloy. Compd. **870**, 159466 (2021)
162. Wu, Y., et al.: Mxene-modulated dual-heterojunction generation on a metal-organic framework (MOF) via surface constitution reconstruction for enhanced photocatalytic activity. Chem. Eng. J. **390**, 124519 (2020)
163. Tu, X., et al.: Mxene/carbon nanohorn/β-cyclodextrin-metal-organic frameworks as high-performance electrochemical sensing platform for sensitive detection of carbendazim pesticide. J. Hazard. Mater. **396**, 122776 (2020)